Nickel based active materials for the high performance supercapacitor

Ik-Hee Kim

Department of Chemical Engineering
School of Molecular Sciences

Graduate School of UNIST

2016

Nickel based active materials for the high performance supercapacitor

Ik-Hee Kim

Department of Chemical Engineering
School of Molecular Sciences

Graduate School of UNIST

Nickel based active materials for the high performance supercapacitor

A dissertation
submitted to the Graduate School of UNIST
in partial fulfillment of the
requirements for the degree of
Master of Science

Ik-Hee Kim

12. 10. 2015
Approved by

Advisor
Ji-Hyun Jang

Nickel based active materials for the high performance supercapacitor

Ik-Hee Kim

This certifies that the dissertation of Ik-Hee Kim is approved.

12. 10. 2015

Signature

Advisor: Ji-Hyun Jang

Signature

Myung Soo Lah

Signature

Hyunhyub Ko

Contents

Abstract

The MOF(Metal-organic Frameworks) was used as a active material of supercapacitor. The Ni-*aph*-MOF was deposited on the nickel plate by using slurry with binder. The capacitance of Ni-*aph*-MOF was showed high performance due to its high surface area and easily intercalatable molecular structure. And the performance of $Ni(OH)_2$ based supercapacitor was enhanced by using current collector. The ultra-thin $Ni(OH)_2$ active layer was deposited on the hierarchical current collector by the electrodeposition method. The improved properties of the supercapacitor can be attributed to the following factors. First, the 3D-current collector increases the effective surface area for the active material, which increases the capacitance value. Second, the electron pathway from $Ni(OH)_2$ to the current collector was decreased by using the thin layered active material, which improves the rate capability by decreasing the internal resistance of the device.

List of Figures

List of Tables

1. Introduction of Supercapacitor.

1.1 Supercapacitor : electrochemical energy storage and conversion system

The supercapacitors also kwon as electrochemical capacitors(ES), have been increasing attracted attentions due to their long cycle stabilities, high power densities and fast charging/discharging rates[1]. With these advantages, supercapacitors have become competitive candidates of storage of the generated electrical energy, electric and hybrid cars and other many portable electric devices[2,3,4]. The supercapacitors can be classified in two different types which are based on their mechanism of charge storage system. The one is EDLC and another is pseudocapacitor.

The capacitive performance of the supercapacitors is determined by the properties of the active material such as electrochemical activities, kinetic features and the surface area[5,6]. The endemic properties of the material cannot be changed but the surface area can be changed by using the various structured current collectors. By using the 3D structured current collector, the surface area of the active material can be dramatically increased[7,8,9,10]. If the amount of loaded active material is same, the one which surface area is large shows high capacitive performance.

1.2 EDLCs (Electrical Double-Layered Capacitors)

One of the supercapacitors is electrical double-layered capacitors, which called as EDLCs. At the early studies, researches of the supercapacitors were focused on the EDLCs. The EDLCs use the carbon based material such as graphene oxide(GO), graphene, active carbon and etc. Among the carbonaceous materials, 3D structured graphene is comes to the fore as high performance EDLCs[11,12,13]. It provides good mechanical and chemical stability, large surface area and high electrical conductivity. The EDLCs use ion adsorption as a charges storage mechanism. EDLCs come from active materials at the electrode, which is interface between the electrolyte and the carbon particles(figure 1.1). In the charge process for balance of the electrode charge, ions of the electrolyte naturally move to the electrode side to neutralize. While the cations which are in the electrolyte move to the negative electrode, the anions move to the positive electrode[1]. During the discharge process, the reverse processes are occurs. In the charge/discharge process of the EDLCs, there is no charge transfer and faradic reaction at the electrode and electrolyte surfaces. This indicates that the concentration of the electrolyte remains constant at the process of the charge/discharge process.

1.3 Pseudocapacitors

The pseudocapacitors are effective electrochemical storage systems that use the Faradic oxidation/reduction reactions for charging/discharging at the surface of the active materials. The active materials of the pseudocapacitors are usually used transition metal derivatives[2,7,14](metal oxide and metal hydroxide), such as MnO_2, RuO_2, NiO, $Co(OH)_2$ and $Ni(OH)_2$. The pseudocapacitors have high capacitance than EDLCs(<300 F/g), however the rate capability is limited as a result of the slow counter ions transporting into the electrode layers to balance charging during the oxidation/reduction reactions. One important approach to improve the performance of the electrodes at high charging/discharging rates is reducing their charge-transfer resistance and increasing the surface area of the electrode materials. In that sense, 3D structured electrode can be the solution of the low rate capability.

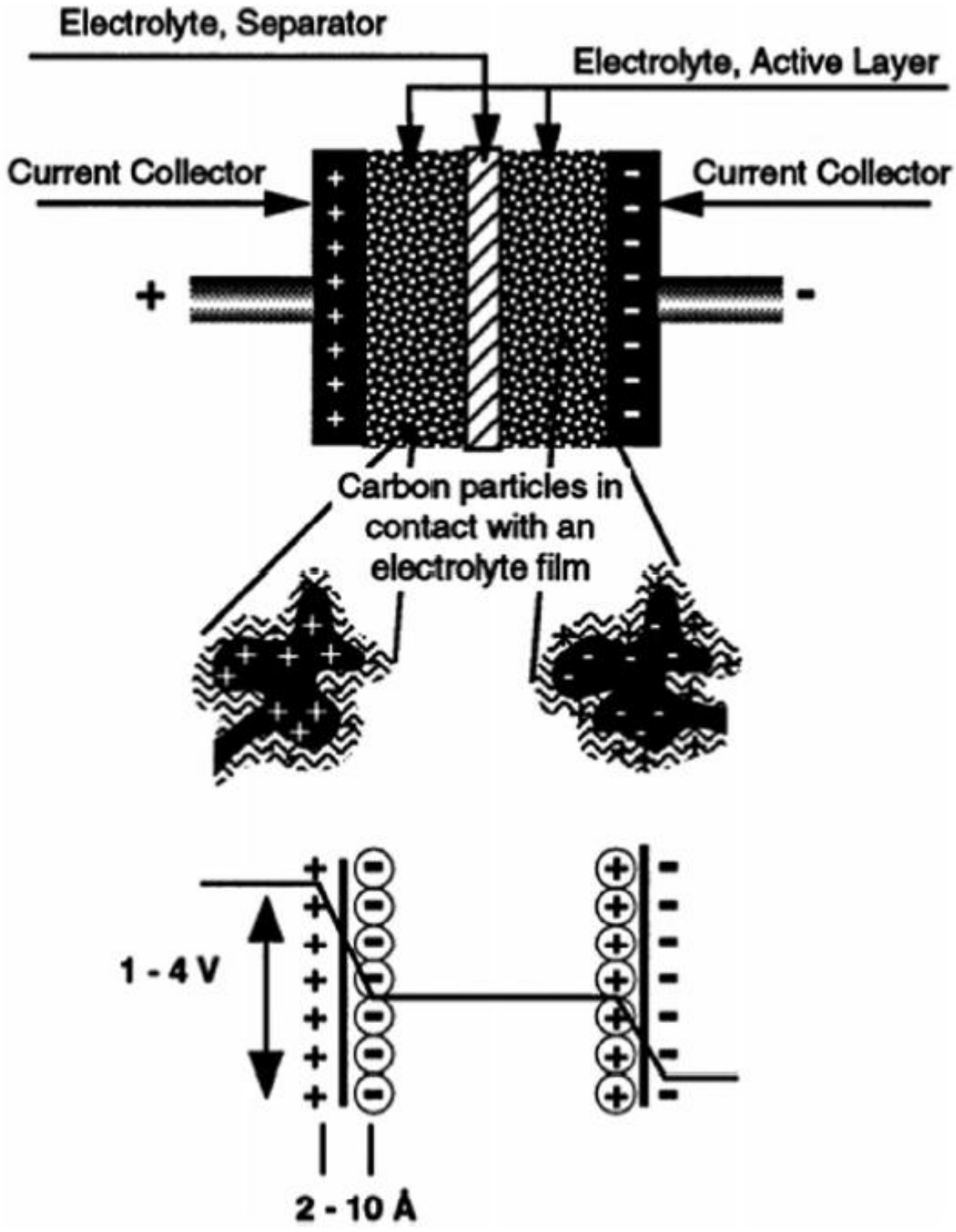

Figure 1.1. "Principles of a single-cell double-layer capacitor and illustration of the potential drop at the electrode/electrolyte interface."

1.4 References

1. Wang, G.; Zhang, L.; Zhang, J., A review of electrode materials for electrochemical supercapacitors. *Chemical Society reviews* **2012,** *41* (2), 797-828.
2. Yeager, M. P.; Su, D.; Marinkovic, N. S.; Teng, X., Pseudocapacitive NiO Fine Nanoparticles for Supercapacitor Reactions. *Journal of the Electrochemical Society* **2012,** *159* (10), A1598-A1603.
3. Meng, F.; Fang, Z.; Li, Z.; Xu, W.; Wang, M.; Liu, Y.; Zhang, J.; Wang, W.; Zhao, D.; Guo, X., Porous Co3O4 materials prepared by solid-state thermolysis of a novel Co-MOF crystal and their superior energy storage performances for supercapacitors. *Journal of Materials Chemistry A* **2013,** *1* (24), 7235.
4. Zhu, X.; Dai, H.; Hu, J.; Ding, L.; Jiang, L., Reduced graphene oxide–nickel oxide composite as high performance electrode materials for supercapacitors. *Journal of Power Sources* **2012,** *203*, 243-249.
5. Liang, K.; Tang, X.; Hu, W., High-performance three-dimensional nanoporous NiO film as a supercapacitor electrode. *Journal of Materials Chemistry* **2012,** *22* (22), 11062.
6. Kim, J. H.; Kang, S. H.; Zhu, K.; Kim, J. Y.; Neale, N. R.; Frank, A. J., Ni-NiO core-shell inverse opal electrodes for supercapacitors. *Chemical communications* **2011,** *47* (18), 5214-6.
7. Yang, G. W.; Xu, C. L.; Li, H. L., Electrodeposited nickel hydroxide on nickel foam with ultrahigh capacitance. *Chemical communications* **2008,** (48), 6537-9.
8. Kundu, M.; Liu, L., Direct growth of mesoporous MnO2 nanosheet arrays on nickel foam current collectors for high-performance pseudocapacitors. *Journal of Power Sources* **2013,** *243*, 676-681.
9. Huang, H.; Tang, Y.; Xu, L.; Tang, S.; Du, Y., Direct formation of reduced graphene oxide and 3D lightweight nickel network composite foam by hydrohalic acids and its application for high-performance supercapacitors. *ACS applied materials & interfaces* **2014,** *6* (13), 10248-57.
10. Zheng, C.; Zhang, J.; Zhang, Q.; You, B.; Chen, G., Three dimensional Ni foam-supported graphene oxide for binder-free pseudocapacitor. *Electrochimica Acta* **2015,** *152*, 216-221.
11. Yoon, J.-C.; Lee, J.-S.; Kim, S.-I.; Kim, K.-H.; Jang, J.-H., Three-Dimensional Graphene Nano-Networks with High Quality and Mass Production Capability via Precursor-Assisted Chemical Vapor Deposition. *Scientific reports* **2013,** *3*.
12. Liu, C.; Yu, Z.; Neff, D.; Zhamu, A.; Jang, B. Z., Graphene-based supercapacitor with an ultrahigh energy density. *Nano letters* **2010,** *10* (12), 4863-8.
13. Guo, C. X.; Li, C. M., A self-assembled hierarchical nanostructure comprising carbon spheres and graphene nanosheets for enhanced supercapacitor performance. *Energy & Environmental Science* **2011,** *4* (11), 4504.
14. Liu, T.; Xu, S.; Wang, L.; Chu, J.; Wang, Q.; Zhu, X.; Bing, N.; Chu, P. K., Miniature supercapacitors composed of nickel/cobalt hydroxide on nickel-coated silicon microchannel plates. *Journal of Materials Chemistry* **2011,** *21* (47), 19093.

2. MOF based supercapacitors

The metal-organic frameworks(MOFs) are porous crystalline materials with multiple functions. Most researches in this area during the past decades have focused on preparing new structured MOFs and exploiting their applications in gas and energy storage, gas separation and catalysis[1, 2]. Other usages of MOFs have rarely been reported[3, 4]. The MOFs have been recently suggested as promising materials for the pseudocapacitiors[5, 6, 7] due to the guaranteed high surface area and high catalytic properties of supercapacitors. Cost-efficient MOFs with great performance as a active material in supercapacitors will present a promising potential in supercapacitors.

2.1. Experimental details and characterization

2.1.1. Synthesis of the Ni-*aph*-MOF

The Ni-aph-MOF was prepared via a hydrothermal method using a 0.33 mmol of $NiCl_2$•6(H_2O) in MeOH and mixed with 1 mmol of adipic acid in DMAc. The solution was heated in a Teflon liner in an autoclave at 120 ℃ 24h. Bright green colored powders were formed, which was filtered with MeOH and washed.

2.1.2. Electrochemical measurement

The electrochemical performance of the Ni-aph-MOF was investigated with conventional three-electrode system using electrochemical workstation (VMP3, Bio-Logic, France) with 1 M KOH solution as the electrolyte. The as-prepared working electrode including Ni-aph-MOF was prepared using a slurry coating procedure. A weight ratio of working electrode was 80 : 10 : 10 of as synthesized material, acetylene black and poly(vinyl difluoride) (PVDF) dissolved in N-methyl-2-pyrrolidone (NMP) were thoroughly mixed together and directly pasted onto flexible nickel steel plate. The electrochemical performances of prepared electrode were examined by cyclic voltammetry and electrochemical galvanostatic charge-discharge tests. The specific capacitance was calculated from following equation, Cs (F /g) $I\Delta t/\Delta Em$, where I is the loaded current (A), Δt is the discharge time (s), ΔE is the potential change during discharge process, and m is the mass of active materials (g)

2.2 Result and Discussion

The figure 2.1 shows a schematic diagram for the synthesis of Ni-*aph*-MOF. The Ni-*aph*-MOF was

synthesized by mixing 0.36 mM of $Ni(Cl)_2 \cdot 6(H_2O)$ in methanol and 1 mM of adipic acid in DMAc(dimethylacetamide). Nickel was chosen as a metal precursor of MOF due to cost-effectiveness, good stability and electrocatalytic property. Heating the solution at 120 ^oC for 24 h in the autoclave results in rod shaped greenish Ni-aph-MOFs(Figure 2.2). The SEM(scanning electron microscopy) images shows the clear rod shaped Ni-*aph*-MOF. It is rod-shaped structures with width of 500 nm and length of 10 um as shown in figure 2. The BET(Brunauer, Emmett and Teller) data(Figure 2.3 and Table 2.1) confirms that the surface area, total pore volume and mean pore size of Ni-*aph*-MOf are 264.10 m^2/g, 0.989 cm^3/g and 7.64 nm, respectively. The XRD(X-ray Diffraction) patterns(Figure 2.4) shows the Ni-*aph*-MOF has clear crystalinity, which has same patterns with simulated XRD patterns. And the stability of the Ni-aph-MOF was tested with the XRD. 1 month after the XRD of same sample was taken. The intensities were decreased but the distinctive peaks were still remained. The Figure 2.5 shows the electrochemical performance of the Ni-*aph*-MOF as active materials for supercapacitors measured in an 1 M aqueous KOH electrolytes. The CV(Cyclic voltammetry) of as-prepared Ni-*aph*-MOF were obtained at different scan rate from 1 mV/s to 100 mV/s and the highest specific capacitance was 973 F/g at a 1 mV/s scan rate(Figure 5a). The CV shows the clear pseudocapacitive behaviour of Ni-aph-MOF that the faradic oxidation/reduction reactions were occurred at the Ni-aph-MOF surface. These CVs correspond to the coupling of MOFs with the OH^- similar to reaction of $Ni(OH)_2$ which is already reported. As shown in table 2.1, the obtained highest specific capacitance at the scan rate of 1 mV/s was 973 F/g and at the current densities of 2 A/g was 736 F/g(Figure 5b). Even at the relatively high current density of 20 A/g, 600 F/g(81 %) of capacitance was well remained(Figure 5c).

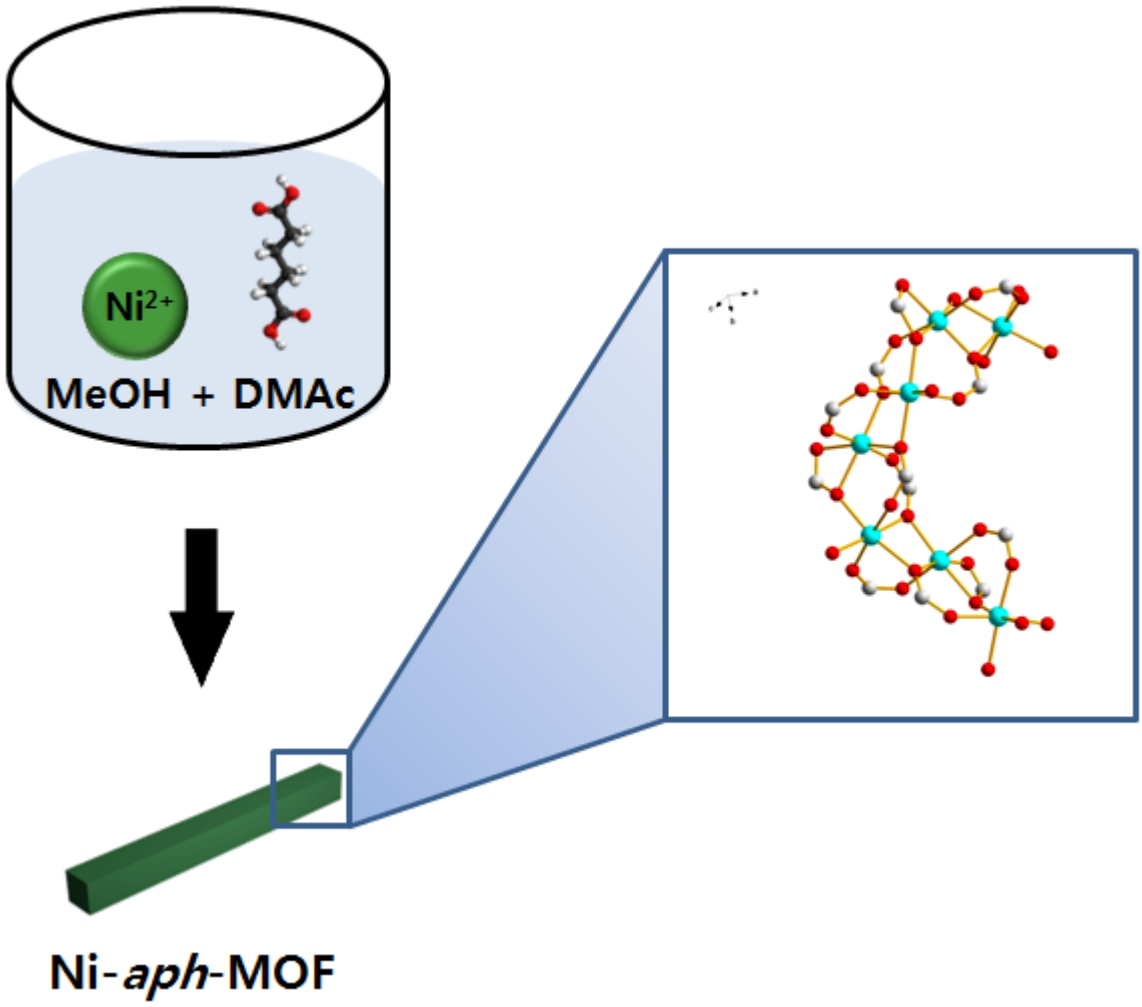

Figure 2.1 A simple schematic diagram of the synthetic process of Ni-*aph*-MOF

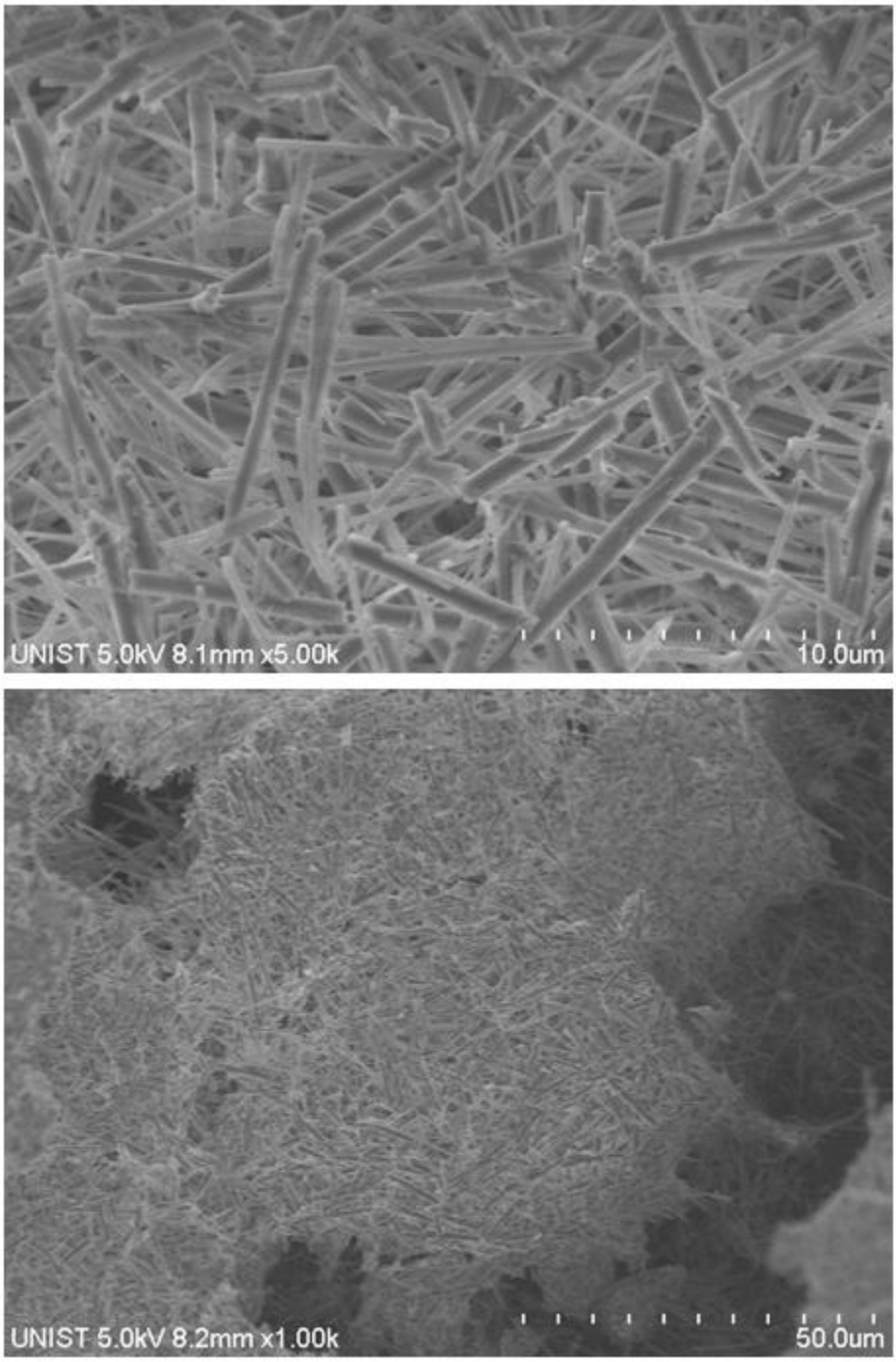

Figure 2.2. Morphological characterization of Ni-aph-MOF

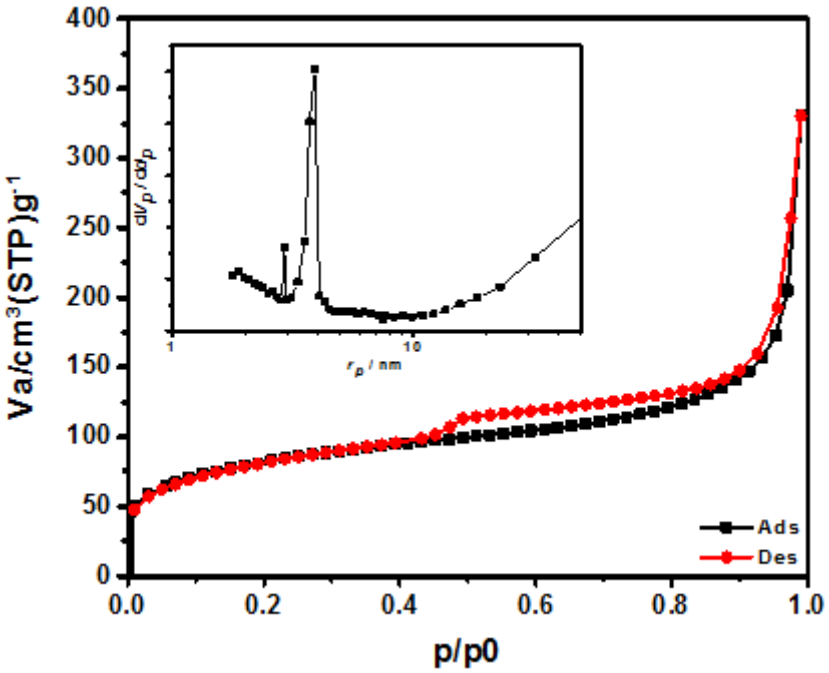

Figure 2.3. BET (Brunaure, Emmett and Teller) analysis of Ni-*aph*-MOF and the insets indicate the BJH pore distribution curve.

	Surface area (m^2g^{-1})	Pore volume (cm^3g^{-1})	Mean pore size (nm)
Ni-*aph*-MOF	264.10	0.989	7.64

Table 2.1. BET surface area, pore volume and mean pore size of Ni-*aph*-MOF

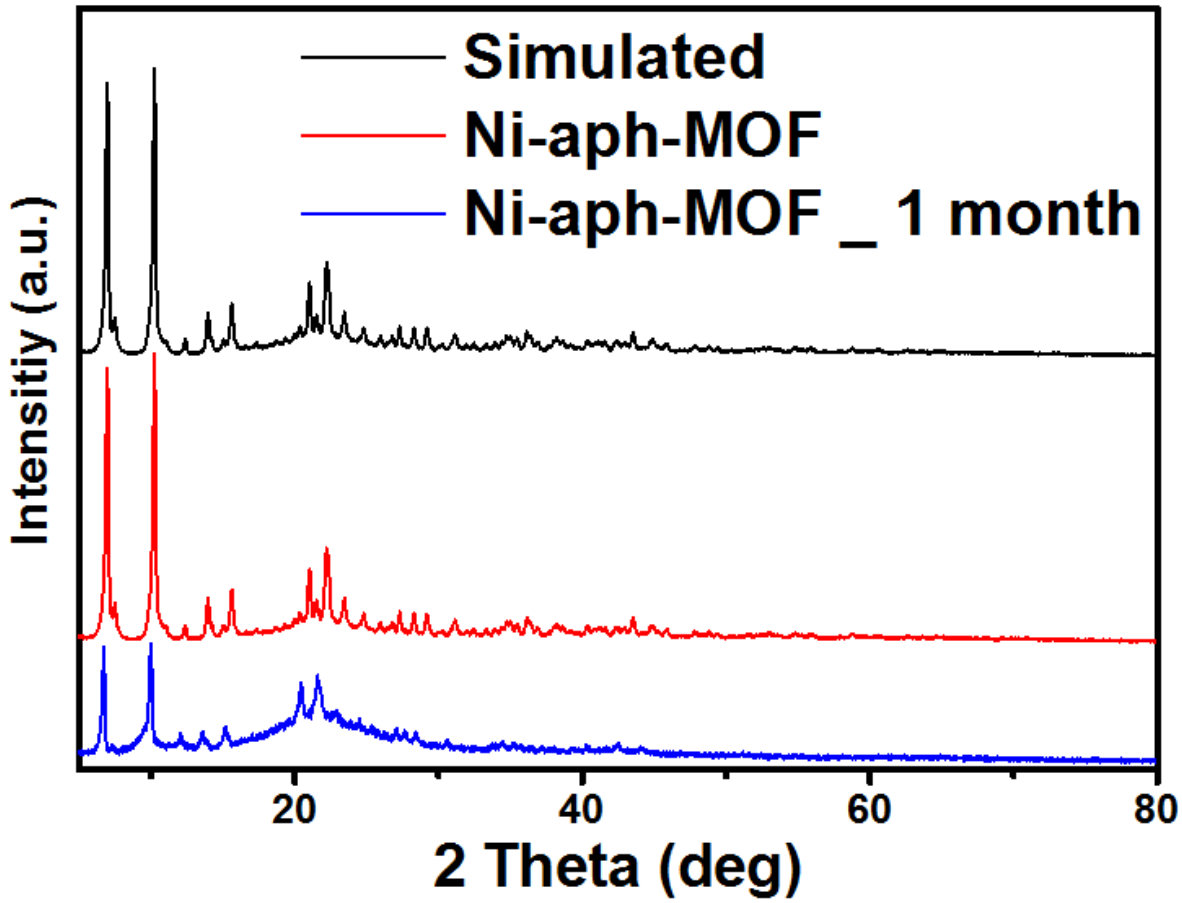

Figure 2.4. The XRD patterns of simulated MOF, synthesized Ni-*aph*-MOF and its stability test.

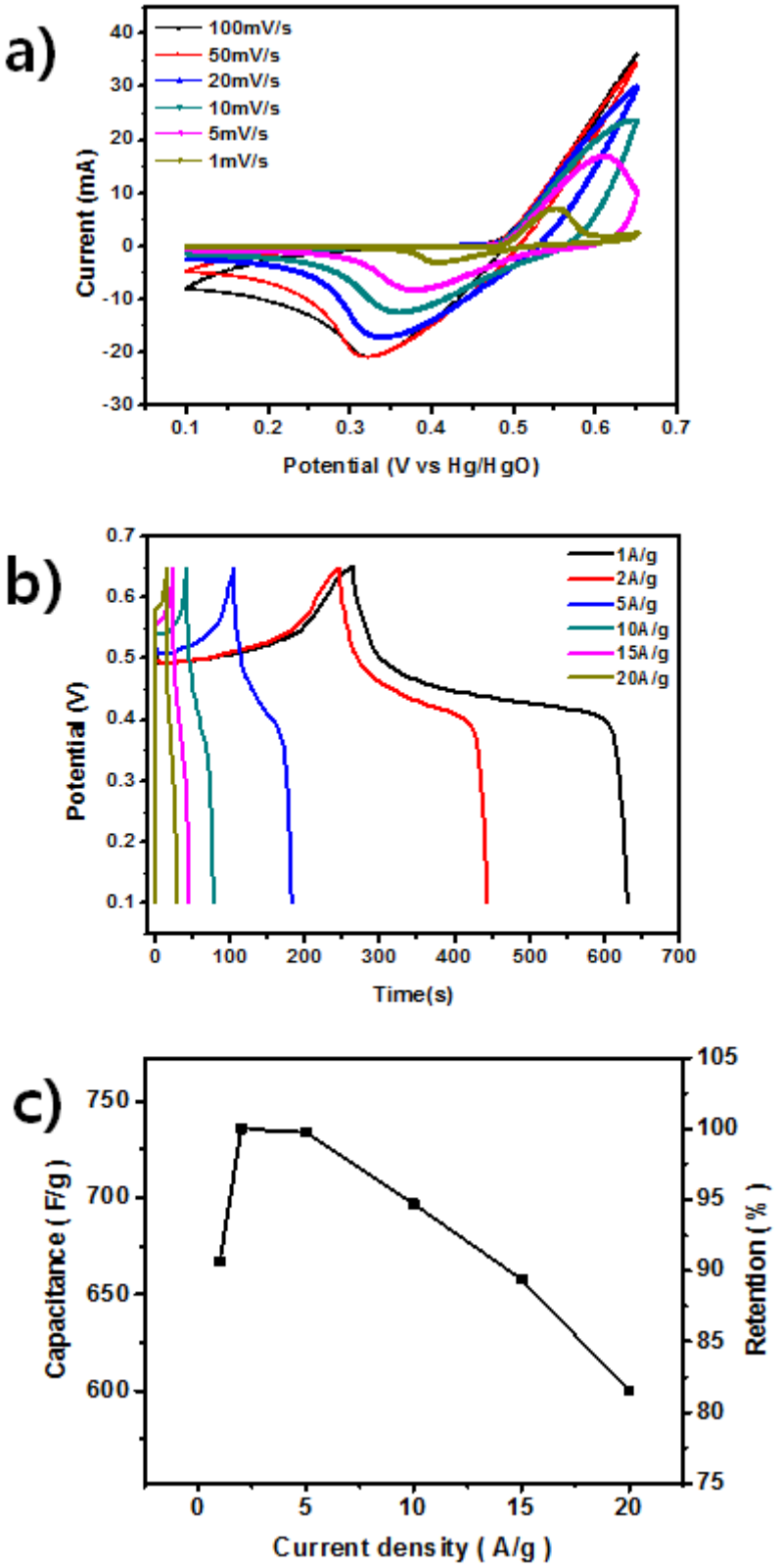

Figure 2.5. The CV(Cyclic voltammetry) and CD(charge/discharge) curves of the Ni-*aph*-MOF versus Hg/HgO reference electrode and Pt counter electrode in the KOH of 1 M.

2.3 Conclusion

We have shown the good performance of the MOF used as a supercapacitor. The MOF based supercapacitor which is Ni-*aph*-MOF showed high specific capacitance of 973 F/g at a scan rate of 1 mV/s and 736 F/g at a current density of 2 A/g. And rate capability of Ni-*aph*-MOF was retained over 80 % at the current density of 20 A/g. The Ni-aph-MOF showed performance at the capacitance and especially rate capability property, due to its high surface area which is electrolyte can well intercalate into the MOF structure.

2.4 References

1. Kumar, P.; Bansal, V.; Deep, A.; Kim, K.-H., Synthesis and energy applications of metal organic frameworks. *Journal of Porous Materials* **2015,** *22* (2), 413-424.
2. Jiang, H. L.; Xu, Q., Porous metal-organic frameworks as platforms for functional applications. *Chemical communications* **2011,** *47* (12), 3351-70.
3. Murray, L. J.; Dinca, M.; Long, J. R., Hydrogen storage in metal-organic frameworks. *Chemical Society reviews* **2009,** *38* (5), 1294-314.
4. Montney, M. R.; Krishnan, S. M.; Supkowski, R. M.; LaDuca, R. L., Diverse entangled metal-organic framework materials incorporating kinked organodiimine and flexible aliphatic dicarboxylate ligands: synthesis, structure, physical properties, and reversible structural reorganization. *Inorganic chemistry* **2007,** *46* (18), 7362-70.
5. Liu, B.; Shioyama, H.; Jiang, H.; Zhang, X.; Xu, Q., Metal–organic framework (MOF) as a template for syntheses of nanoporous carbons as electrode materials for supercapacitor. *Carbon* **2010,** *48* (2), 456-463.
6. Yang, J.; Zheng, C.; Xiong, P.; Li, Y.; Wei, M., Zn-doped Ni-MOF material with a high supercapacitive performance. *J. Mater. Chem. A* **2014,** *2* (44), 19005-19010.
7. Yang, J.; Xiong, P.; Zheng, C.; Qiu, H.; Wei, M., Metal–organic frameworks: a new promising class of materials for a high performance supercapacitor electrode. *J. Mater. Chem. A* **2014,** *2* (39), 16640-16644.

3. High capacitive $Ni(OH)_2$ supercapacitor supported on a hierarchical current collector

As mentioned before, 3D structure can be the alternative method to improve performance of the supercapacitors. Compared with 2D current collector, 3D structured current collector is provided increase of the effective surface area when the same amount of active material is loaded. And increased surface area induces the increase of capacitance[1, 2, 3]. Due to inducement property of thinner active material of 3D current collector[4, 5, 6, 7], the thickness of the active material depends on the surface area of the current collector. Therefore the studies about the current collectors should be achieved the current collector which has larger surface than conventional current collectors.

3.1 Experiment details and characterization

3.1.1 Preparation of various current collectors

All the electrodes were made on the commercial nickel plate.

3.1.1.1 Preparation of Ni plate

The active area of Nickel plates were 1.1 cm by 1 cm. Nickel plates were cleaned at the acidic solution (HCl : H_2O = 1 : 10) for 5 min and washed at the EtOH for 30 min with sonication.

3.1.1.2 Preparation of Ni foam

The Nickel foams were cleaned at the acidic solution (HCl : H_2O = 1 : 10) for 5 min to eliminate the NiO surface layer and washed at the EtOH for 30 min with sonication.

3.1.1.3 Preparation of pCu current collector [8]

The copper deposition solution was prepared $CuSO_4 \cdot 5H_2O$ of 9.98 g with 35 % H_2SO_4 of 8 ml in the D.I. water of 100 ml. The dendritic copper structure was deposited on the cleaned nickel plate at the current density of 3 A/cm^2 for 30 s. Deposited copper was soaked in the glucose solution of concentration of 0.005 M for 1 h. Then the prepared sample was heated in the Ar condition at 500 ^oC for 30 min and cooled fast in the Ar condition.

3.1.1.4 Preparation of pNi current collector

The nickel deposition solution was prepared $CuSO_4 \cdot 5H_2O$ of 2.5 g and with $NiSO_4 \cdot 5H_2O$ of 50 g 35 % H_2SO_4 of 8 ml in the D.I. water of 100 ml. The dendritic copper-nickel structure was deposited on the cleaned nickel plate at the current density of 3 A/cm^2 for 150 s. Deposited pCuNi structure was washed in the H_2O and dried at 60 ^oC for 3 h. Deposited copper was etched in the ammonium persulfate solution of 0.1 M for 0, 1 and 5 min, each and washed in the H_2O. Prepared sample was dried in the oven at 60 ^oC for 12 h.

3.1.2 Deposition of the $Ni(OH)_2$

The $Ni(OH)_2$ deposition solution was prepared in the H_2O with 0.1 M $Ni(NO_3)_2$. As-prepared all the current collectors were deposited same deposition method, at the current density of -11 mA versus Ag/AgCl reference electrode with Pt counter electrode.

3.1.3 Electrochemical measurement

The electrochemical measurements of all the prepared smaples were evaluated using a three-electrode system in 1 M KOH aqueous solution. To confirm the electrochemical properties of the $NiOH)_2$/C/pCu, CV(Cyclic voltammetry) and CD(charge/discharge) measurement were conducted. The CVs and CDs of the $Ni(OH)_2$/C/pCu were measured at the scan rates of from 5 to 50 mV/s and at the current densities of from 1 to 50 A/g versus Hg/HgO reference electrode with Pt counter electrode. And the CVs and CDs of the $Ni(OH)_2$/pNi series were measured at the scan rates of 1 ~ 100 mV/s and at the current densities of 1 ~ 100 A/g. All the samples were measured EIS in the 1 M KOH solution versus reference electrode of Hg/HgO with Pt counter electrode from 100000 Hz to 0.1 Hz.

3.2 Results and Discussion

The morphologies of $Ni(OH)_2$ which are deposited on nickel plate and nickel foam(figure 3.1). As shown in the figure 3.1.a, on the nickel plate, small particles of the $Ni(OH)_2$ were deposited. On the other hand, on nickel foam, film type of the $Ni(OH)_2$ was deposited(figure 3.1.b). To confirm the $Ni(OH)_2$, XRD(X-ray diffraction) was investigated(figure 3.2).The XRD patterns shows the typical $Ni(OH)_2$ patterns (003), (006), (101) and (110) crystal faces.

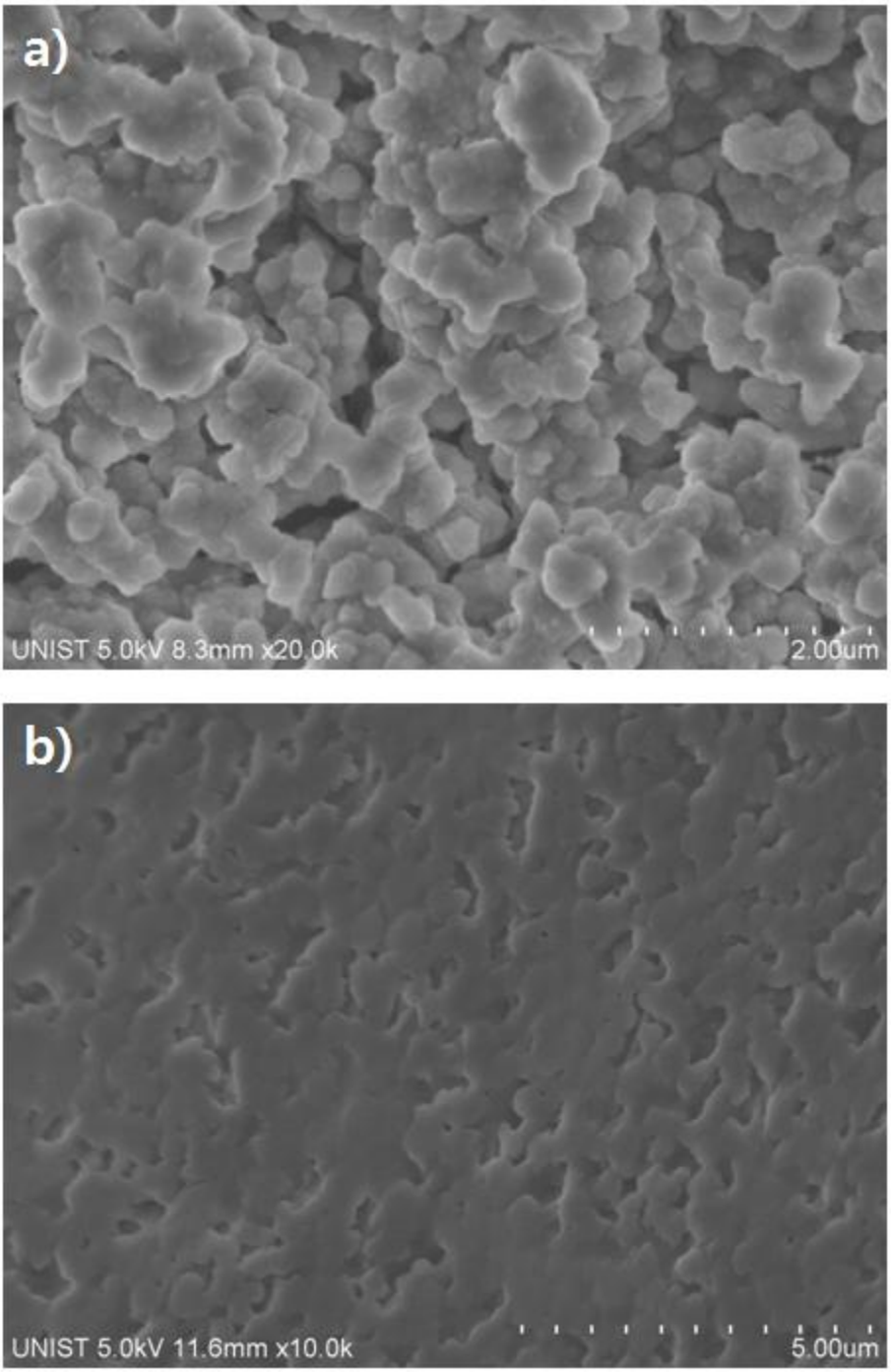

Figure 3.1. SEM images of $Ni(OH)_2$ on (a) nickel plate and (b) nickel foam

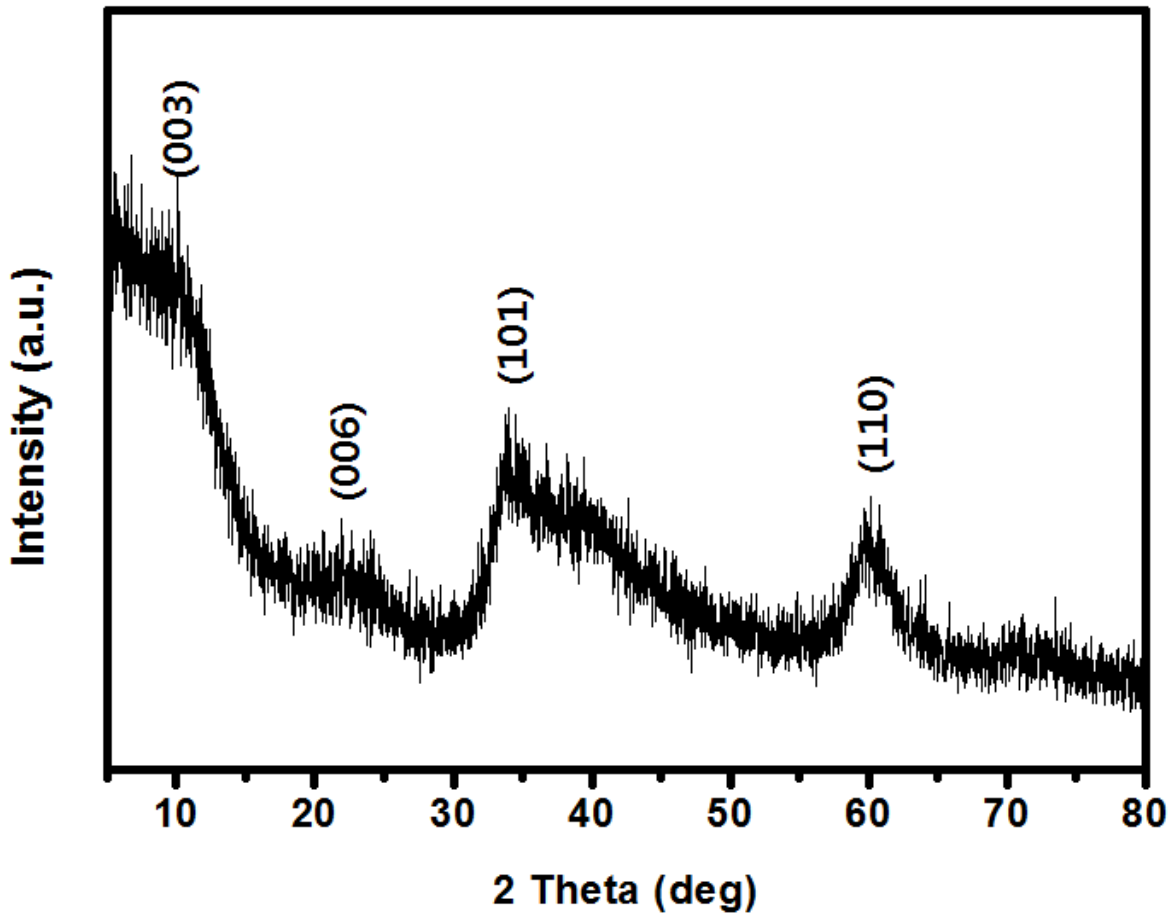

Figure 3.2. XRD patterns of the deposited thin film $Ni(OH)_2$

3.2.1 $Ni(OH)_2$/C/pCu

Simple schematic diagrams of synthesize process of the pCu is shown in the figure 3.3. First the dendritic copper current collector was deposited on the substrate. Then prepared sample was soaked in the glucose solution for 1 h. For the carbonization and reduction, soaked sample was heated at the 500 ^oC for 30 m in the Ar condition. Finally thin film type $Ni(OH)_2$ was deposited on the carbon coated current collector. The morphologies of the pCu and C/pCu(carbon coated pCu) and $Ni(OH)_2$/C/pCu were shown in the figure 3.4. Before carbon coating, the morphology of pCu has typical dendritic structure. When the copper is deposited, bubbles are generated. Due to the large pores which made via the generated bubbles and dendritic structure, effective surface area of the active material has been increased. Low magnification image of the pCu is shown in the figure 3.4.a. Tens of micrometers of the large pores are randomly distributed on the nickel plate and they are consisted of branches with hundreds of nanometers of small particles(figure 3.4.b). And the height of the pCu is 60 ~ 70 micrometers, as shown in the figure 3.4.c. Due to chemical and electrochemical instability of the copper, carbon coating is needed. If do not any process to pCu, it is easily oxidized in the air and basic electrolyte. In the carbon coating process, pCu was soaked in the glucose solution and heated in the Ar condition. During the heating process, structural shrinkage was occurred(figure 3.4.d). Then the thin film of $Ni(OH)_2$ was deposited on the C/pCu, as shown in figure 3.4.e. Thin film $Ni(OH)_2$ was fully covered the C/pCu structure. To confirm the stability of the copper current collector, XRD was investigated(figure 3.5). 3 types of XRD patterns are shown in the figure 3.6., pCu, C/pCu and $Ni(OH)_2$/C/pCu. As shown in the figure 3.6, the surface of the pCu was oxidized to the CuO while the C/pCu was not showing any CuO patterns. However, the $Ni(OH)_2$ patterns could not find in the XRD patterns of $Ni(OH)_2$/C/pCu due to the high background intensity. Therefore to investigate the $Ni(OH)_2$ contents, EDX(Energy Dispersive X-ray Spectroscopy) was taken(figure 3.6). The elemental maps of Cu, C, Ni and O shows a uniformly dispersed dots. These indicate that the carbon and Ni(OH)2 were uniformly well coated on the pCu. Active material of thin film type on the current collector which decrease the electron pathway can reduce the IR loss due to reducing of the total mass of active material and adding any binder(figure 3.7). Figure 3.8.a. shows the CV curves of as-prepared sample at various scan rates. The specific capacitances of the CVs were 1, 2, 3, and 4 at the scan rate of 5, 10, 20 and 50 mV/s. And the specific capacitances of the CDs were 1, 2, 3, 4, 5 and 6 at the current densities of 1, 2, 5, 10, 20 and 50 A/g(figure 3.8.b). The both rate cpability of discharge and areal were remained over 80 %(figure 3.8.c). Also the cyclic performances of discharge and areal capacitances were retained over 80 % to 10000 cycles(figure 3.8.d). As shown in figure 3.9, EIS was measured to support the electrochemical behavior of the $Ni(OH)_2$/C/pCu. The EIS shows the variation of interior electrode resistance and interfacial resistance between the electrode and electrolyte. The

onset on the Z_{real} axis indicates that the intrinsic and electrical contact resistance of the electrode. The semicircle at the high frequency region which is Rct(Charge transfer resistance) caused by Faradic reactions which is Ni^{2+}/Ni^{3+} redox reaction. The straight tail in the medium frequency region is Warburg impedance which is related to the electrolyte diffusion within the electrode. The contact resistances of the $Ni(OH)_2$/nickel plate, $Ni(OH)_2$/nickel foam and $Ni(OH)_2$/C/pCu are 1.94, 32.8 and 1.25 Ω each. It is clear evidence of enhanced conductivity of $Ni(OH)_2$/C/pCu.

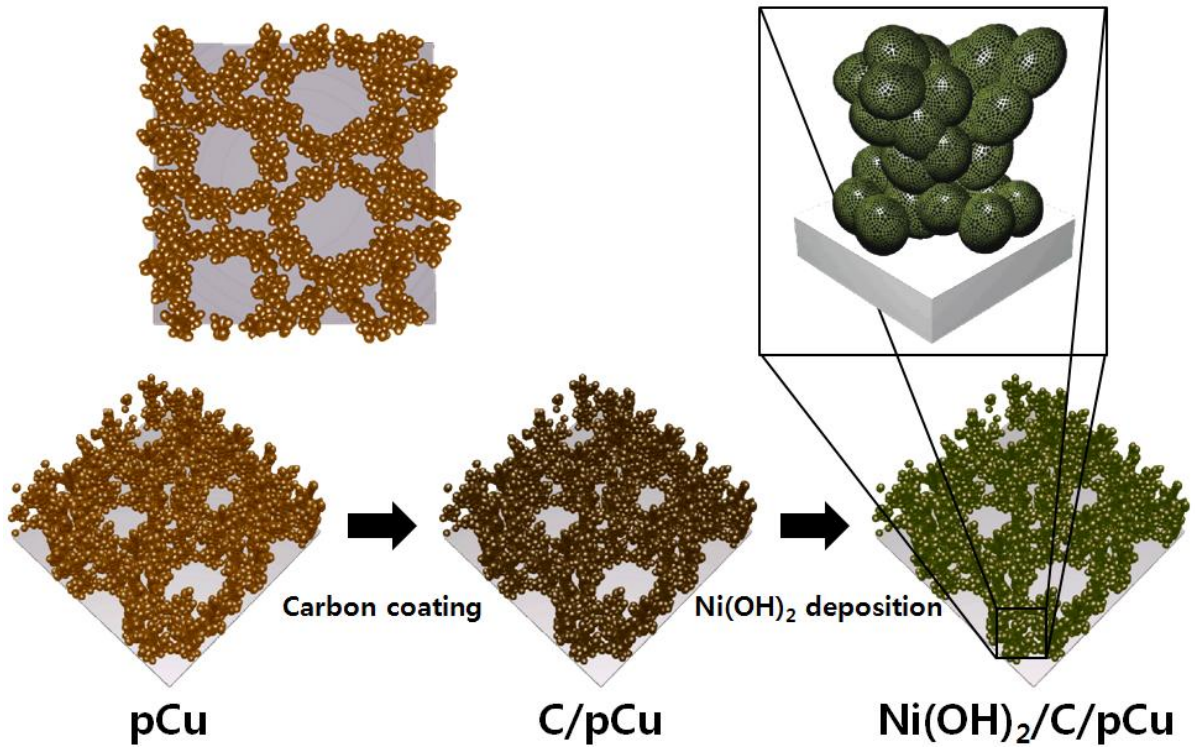

Figure 3.3. A schematic show of the procedure from formation of porous copper substrate to deposition of ultrathin $Ni(OH)_2$ layer on porous copper substrate deposited on nickel plate with carbon coating.

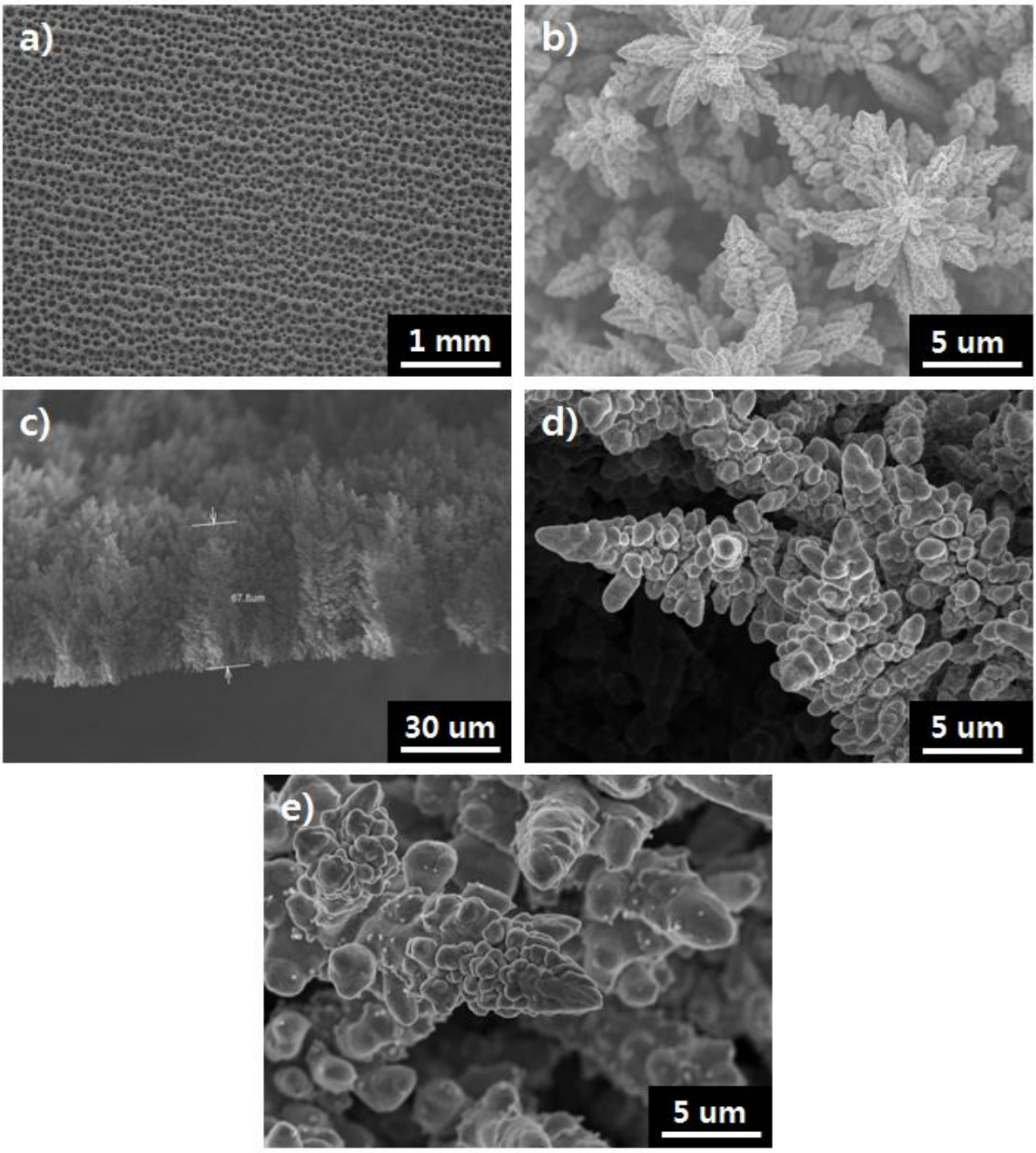

Figure 3.4. SEM images of pCu (a) low magnetic and (b) high magnetic and (d) cross sectional view of pCu. High magnetic images of (d) C/pCu and (e) $Ni(OH)_2$/C/pCu

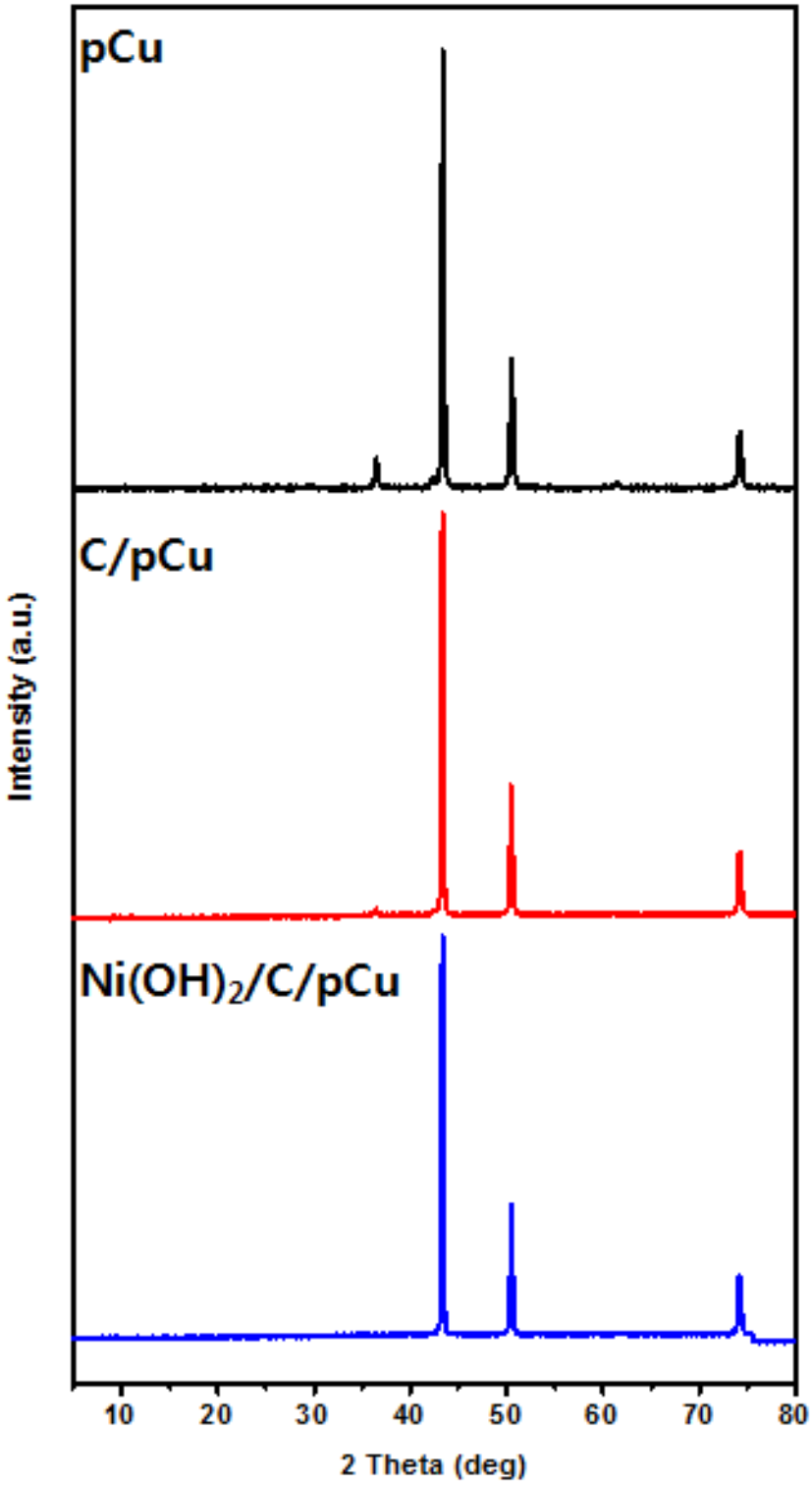

Figure 3.5. XRD patterns of pCu, C/pCu and $Ni(OH)_2$/C/pCu

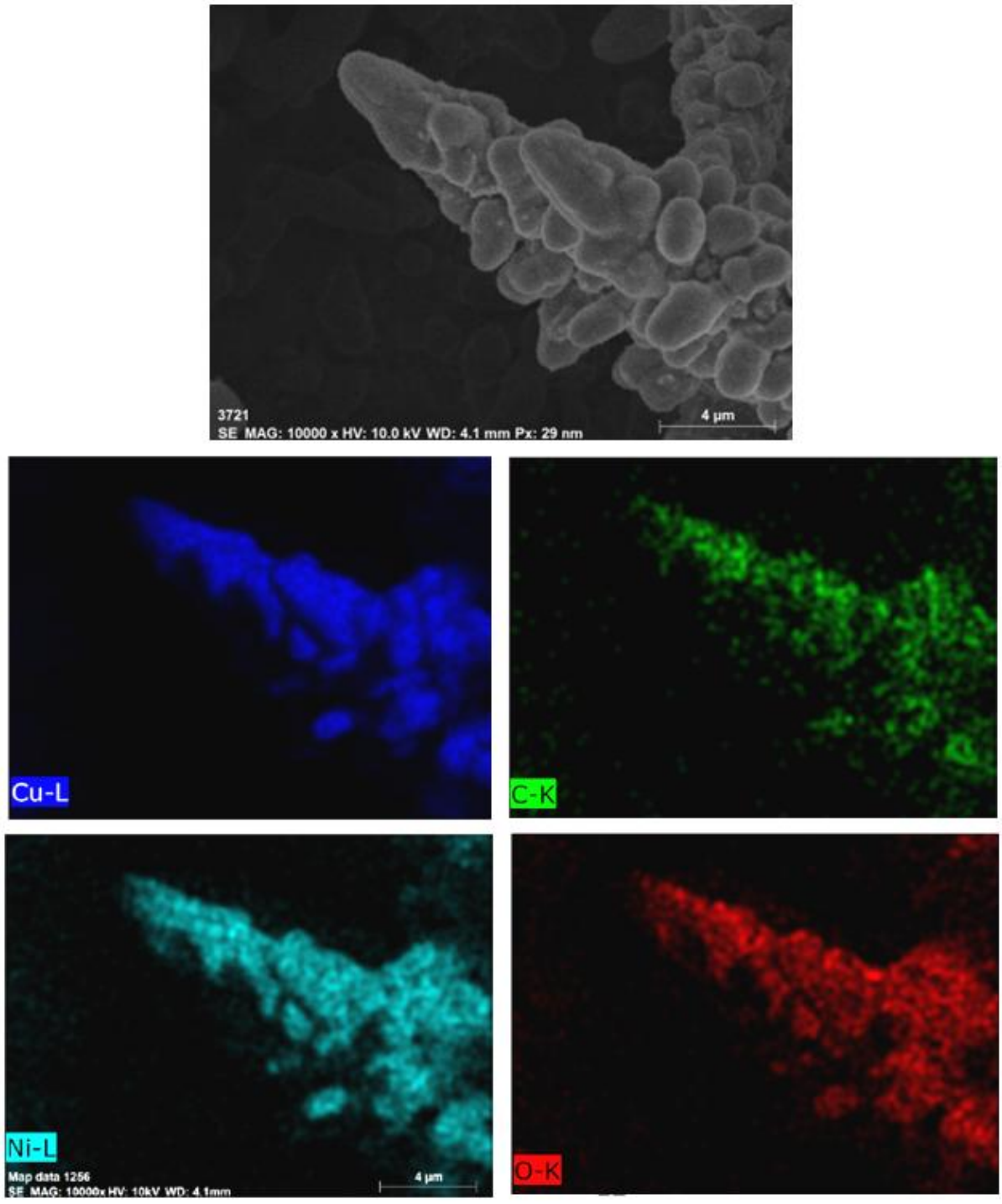

Figure 3.6. EDX mapping of the $Ni(OH)_2$/C/pCu

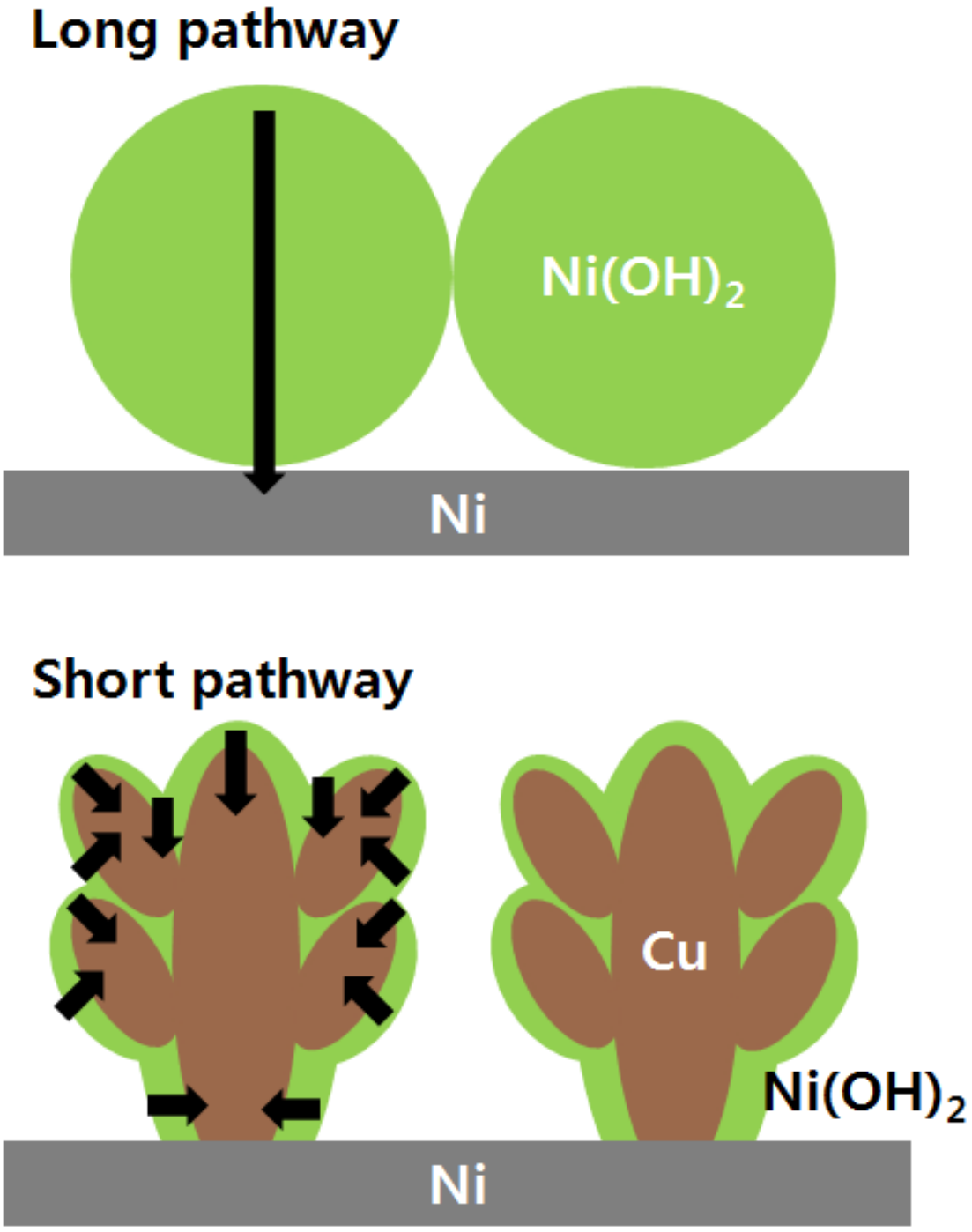

Figure 3.7. Schematic diagram of the electron transfer mechanism comparison between bulk $Ni(OH)_2$ and thin film $Ni(OH)_2$ on 3D copper current collector

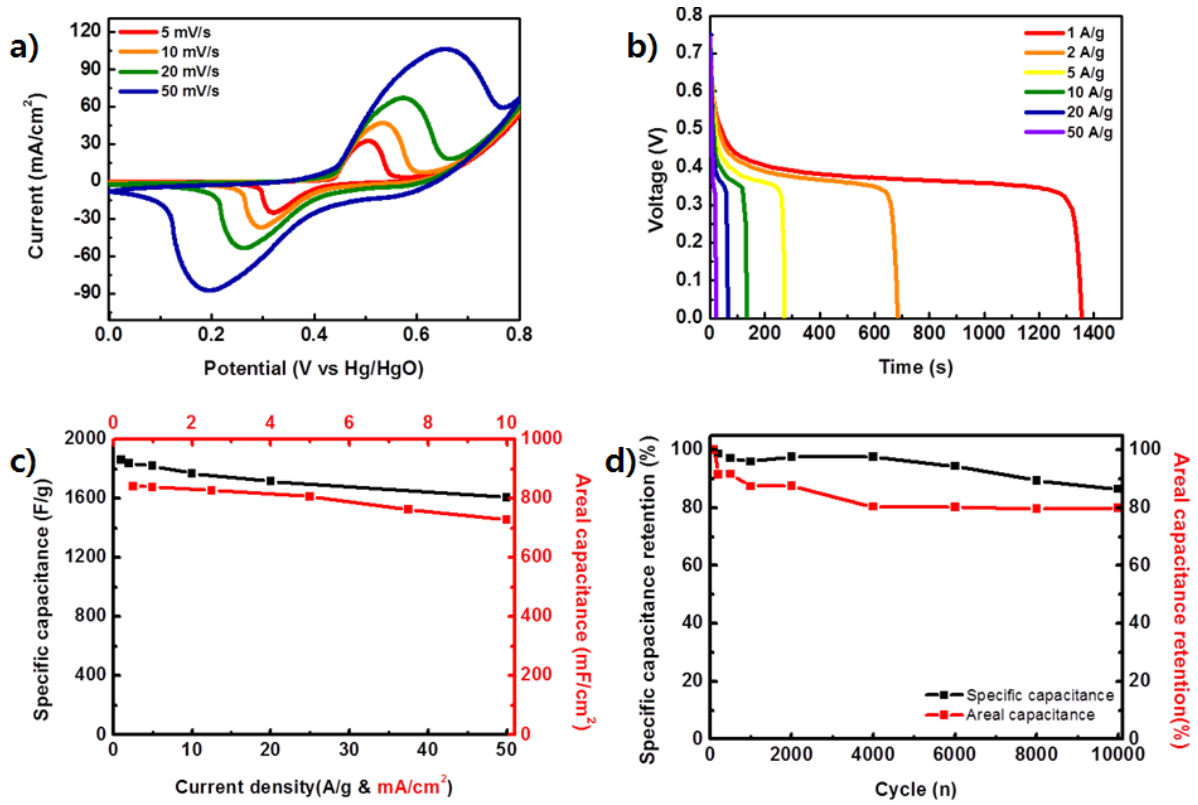

Figure 3.8. Electrochemical characterization of $Ni(OH)_2$/C/pCu with three-electrode system. (a) CV curves in 1 M KOH at various scan rates, (b) discharge curves in the Galvanostatic charge/discharge measurement, (c) rate capability of specific discharge capacitance and areal capacitance and (d) cyclic stability of $Ni(OH)_2$/C/pCu at the current density of 200 A/g and 20 mA/cm^2.

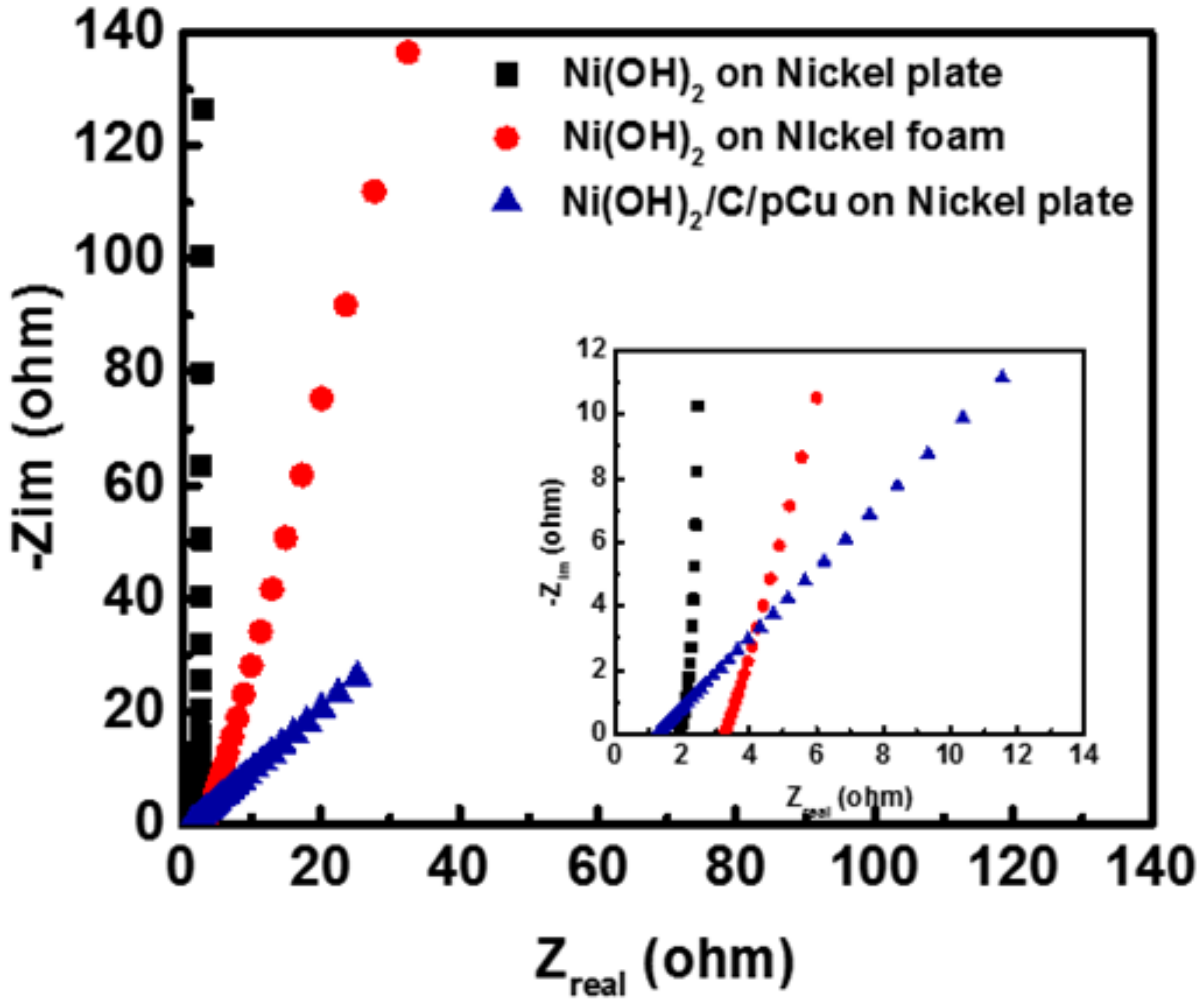

Figure 3.9. Nyquist plot of the $Ni(OH)_2$/nickel plate, $Ni(OH)_2$/nickel foam and $Ni(OH)_2$/C/pCu

3.2.2 $Ni(OH)_2$/pNi

Schematic process of making a 3D nickel current collector structure is shown in the figure 3.10. Similar to the pCu, denritic structure was deposited on the nickel plate which is copper and nickel complexes. Co-deposited pCuNi(figure 3.11.a and b) was used for the current collector itself and etched for the preparation of pNi series. Deposited pCuNi was etched in the ammonium persulfate of 0.1 M for 1 m(pNi_1 figure 3.11.c) and 5 m(pNi_5 figure 3.11.d). After etching process, micro scaled large pores were remained but the small sized particles were converted to flower-like dendritic structure. Due to the removal of copper, surface area of the current collector was largely increased. Then the $Ni(OH)_2$ of thin film type was deposited on the as-prepared pCuNi, pNi_1 and pNi_5(figure 3.12.). Low magnetic SEM image of the pCuNi is similar to pCu, due to the same deposition method. On the other hand, the high magnetic SEM image of the pCuNi is little different to the pCu, due to the co-deposited copper and nickel. The pCuNi has a core-shell like structure, that is the nickel is covered the copper. At the etching process of the pCuNi, first, nickel which is covered the copper is etched. After the copper is exposed to the etching solution, copper is removed intensely from the top side of the current collector. Then the pore size of the current collector is getting bigger, therefore the surface area of the current collector is increase. Remained structure was worked effectively in side of the surface area. To confirm the copper contents of the various current collectors, XRD was investigated. As shown in the figure 3.13, the copper contents of the pNi_5 were intensely decreased compared to the pCuNi. In the XRD patterns of pCuNi, copper peaks were strongly appeared at the 43.3, 50.5 and 74.2 ^{o}. Most of the copper contents were removed in the etching process. Removing of the copper is increasing the capacitor and the surface area. Figure 3.14 and Table 3.1 shows the BET data of the as-prepared samples which are pCuNi, pNi_1 and pNi_5. Figure 3.14 is adsorption/desorption isotherm plots of the pCuNi, pNi_1 and pNi_5 and insets are the pore distributions of the each samples. Due to the etching process, the surface of the pNi_5(2.097 m^2/g) is 2 times larger than the pCuNi(0.907 m^2/g) and pore volume of the pNi(0.0054 cm^3/g) is also 23% larger than pCuNi(0.0044 cm^3/g). CV and CD were measured in the 1.0 M KOH electrolyte versus Hg/HgO reference electrode with Pt counter electrode. Highest specific discharge capacitance of the pNi_5 was ~3637 at the current density of 1 A/g(figure 3.15.c) and the capacitance was retained over 90 %(~3516 F/g) at the current density of 100 A/g. And it is higher capacitance than the pCuNi and pNi_1 both and their rate capabilities were also retained over 90% at the current density of 100 A/g, due to the 3D current collector(figure 3.15.d). The loading mass of the active material on pNi series was should be low(~200 mg) due to the effective surface area of the capacitor. If loading mass of the $Ni(OH)_2$ was over 300 mg, the capacitance and the cyclic performance were dramatically decreased due to the thick active material has long electron pathway and low effective active surface area(figure 3.16) as explained in part of

pCu(figure 3.7). To support the superior capacitance of the pNi_5, EIS was investigated(figure 3.17). The Rs(contact resistance) of pNi_5 is smallest among the as-prepared samples, which are $Ni(OH)_2$/nickel foam, $Ni(OH)_2$/pCuNi, $Ni(OH)_2$/pNi_1 and $Ni(OH)_2$/pNi_5 are 2.40, 1.78, 1.55 and 1.32 Ω each. As same as Rs, pNi_5 has smallest Rct as shown in the inset of figure 3.16.

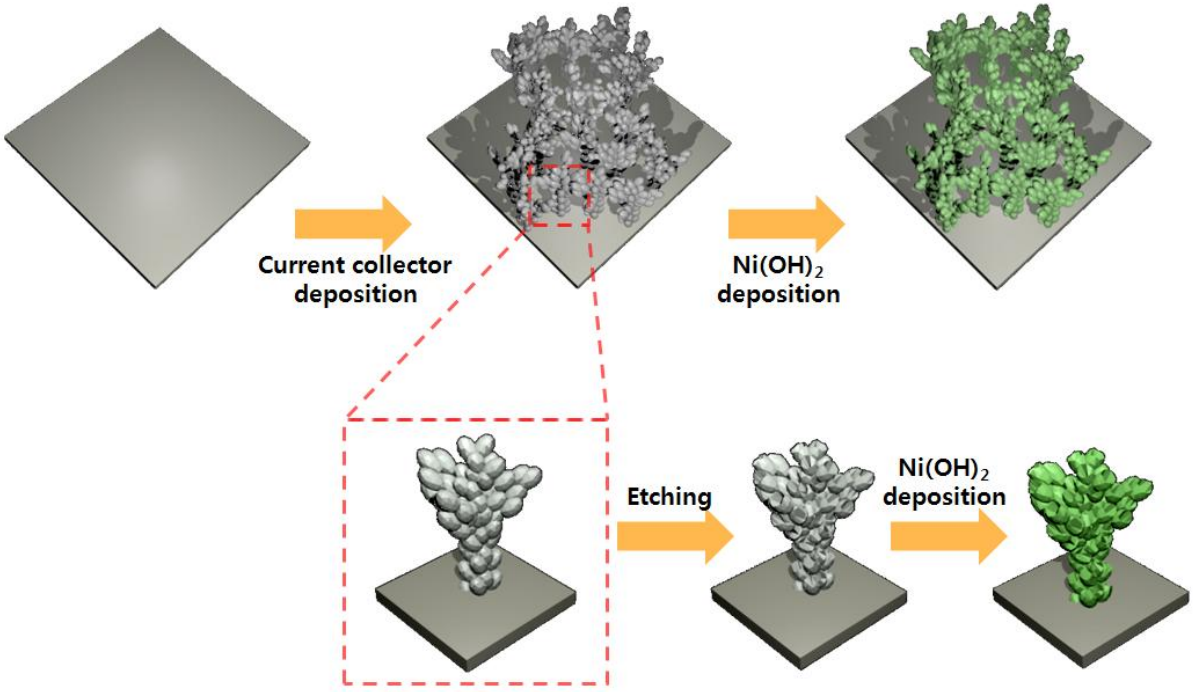

Figure 3.10. Simple process of making a 3D nickel current collector structure

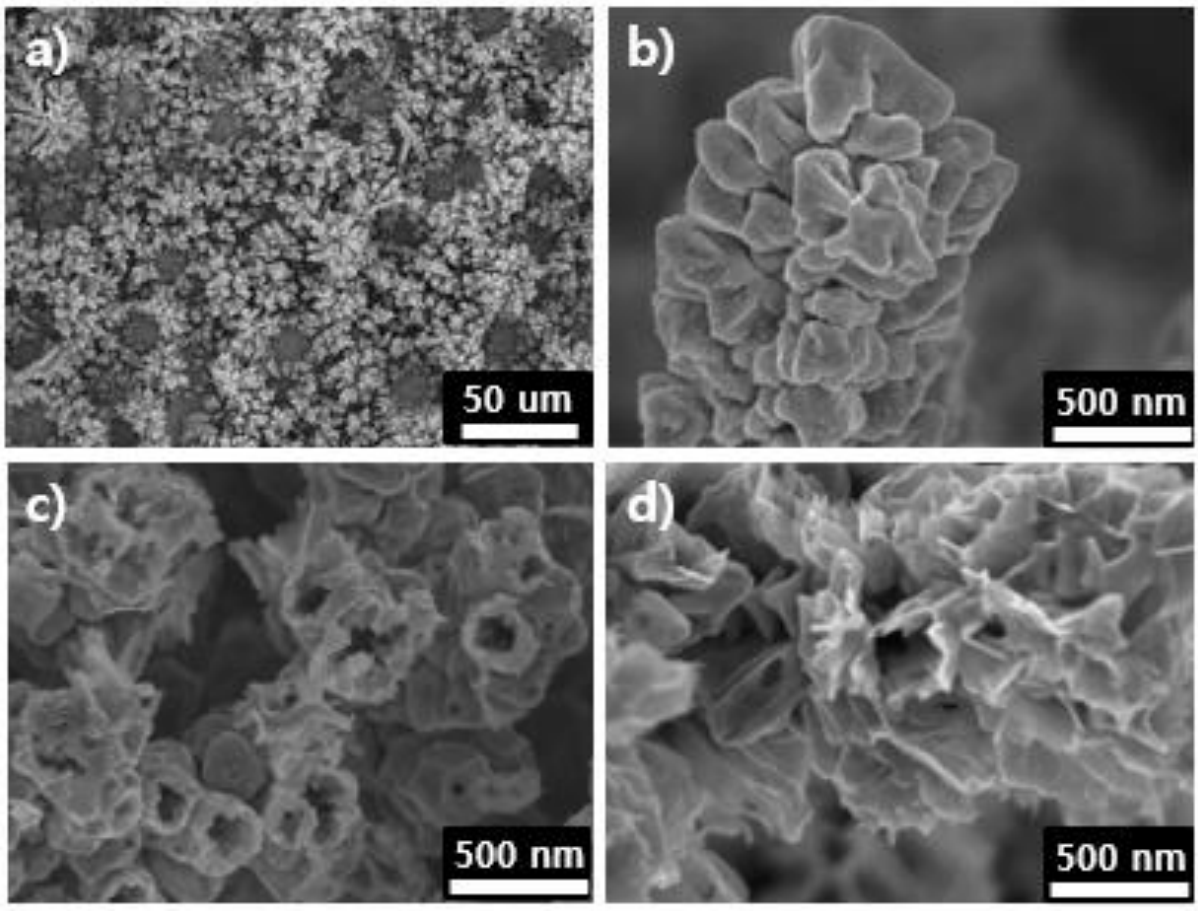

Figure 3.11. SEM images of the pCuNi at the (a) low magnetic and (b) high magnetic, and high magnetic images of (c) pNi_1 and (d) pNi_5

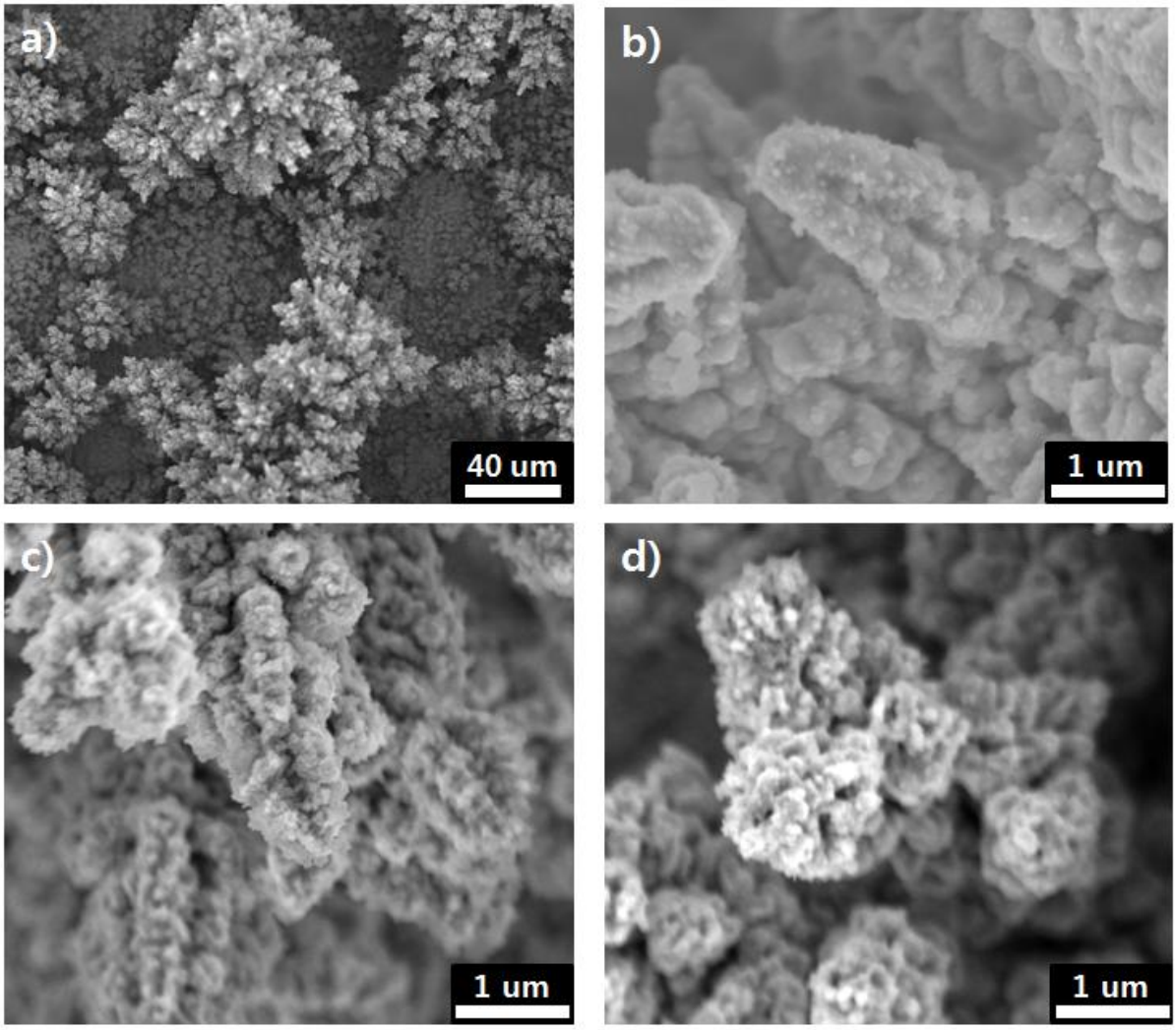

Figure 3.12. Low magnetic SEM image of (a) $Ni(OH)_2$/pCuNi and high magnetic images of (b) $Ni(OH)_2$/pCuNi, (c) $Ni(OH)_2$/pNi_1 and (d) $Ni(OH)_2$/pNi_5

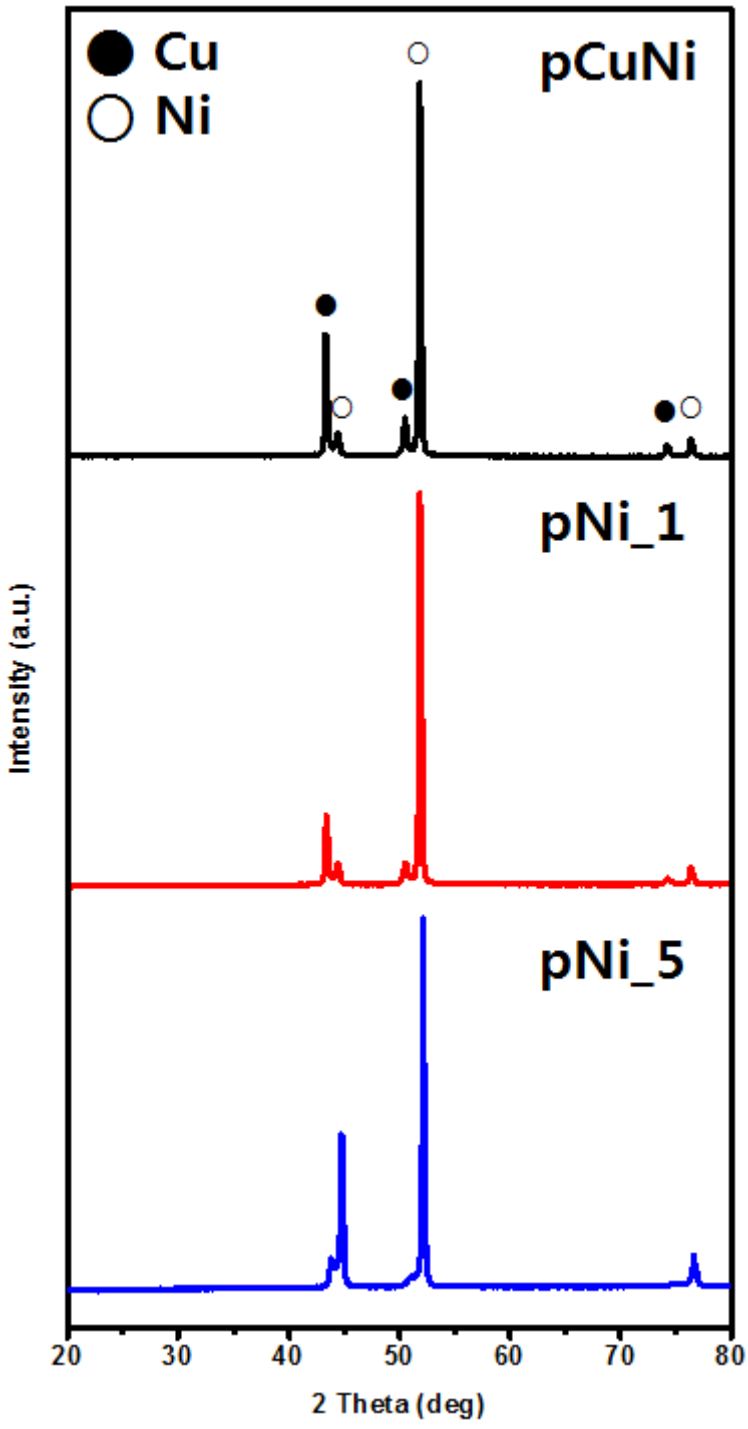

Figure 3.13. XRD of the pCuNi, pNi_1 and pNi_5

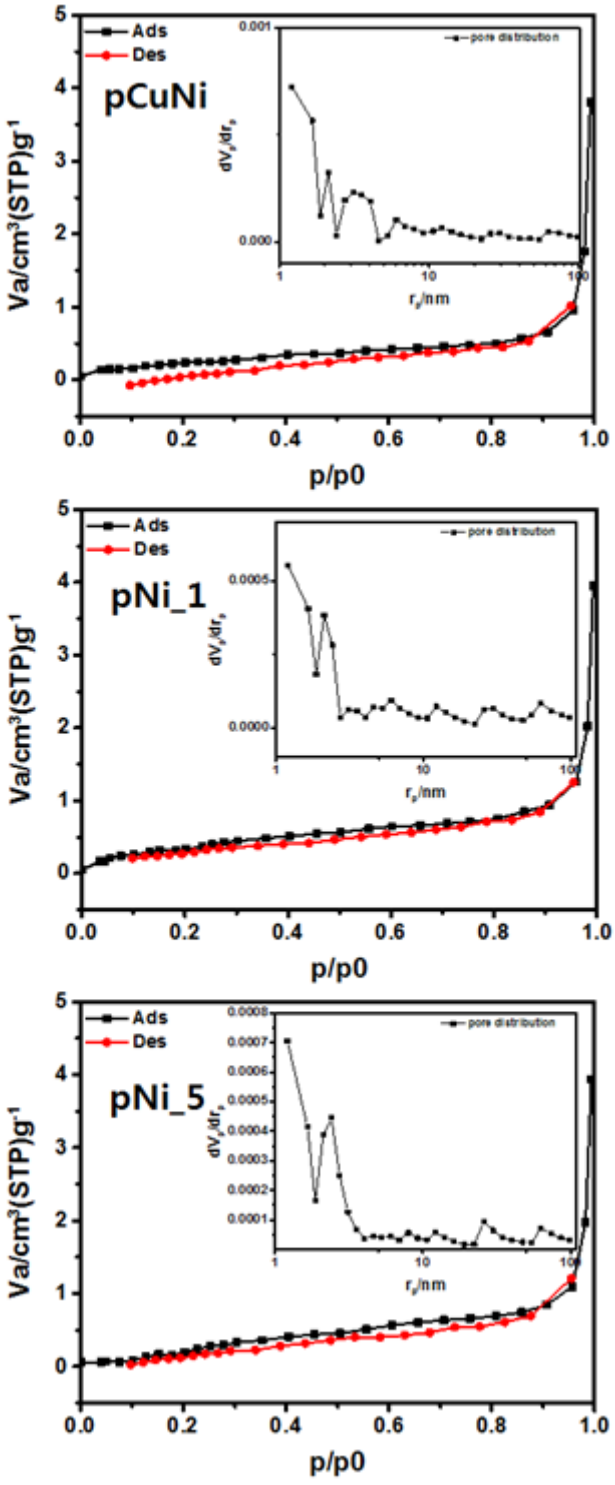

Figure 3.14. BET adsorption/desorption graph of the pCuNi, pNi_1 and pNi_5. The inset is pore distribution.

	Surface area (m^2g^{-1})	Pore volume (cm^3g^{-1})	Mean pore size (nm)
pCuNi	0.907	0.0044	23.70
pNi_1	1.441	0.0050	15.23
pNi_5	2.097	0.0054	9.65

Table 3.1. BET surface area, pore volume and mean pore size of the pCuNi, pNi_1 and pNi_5

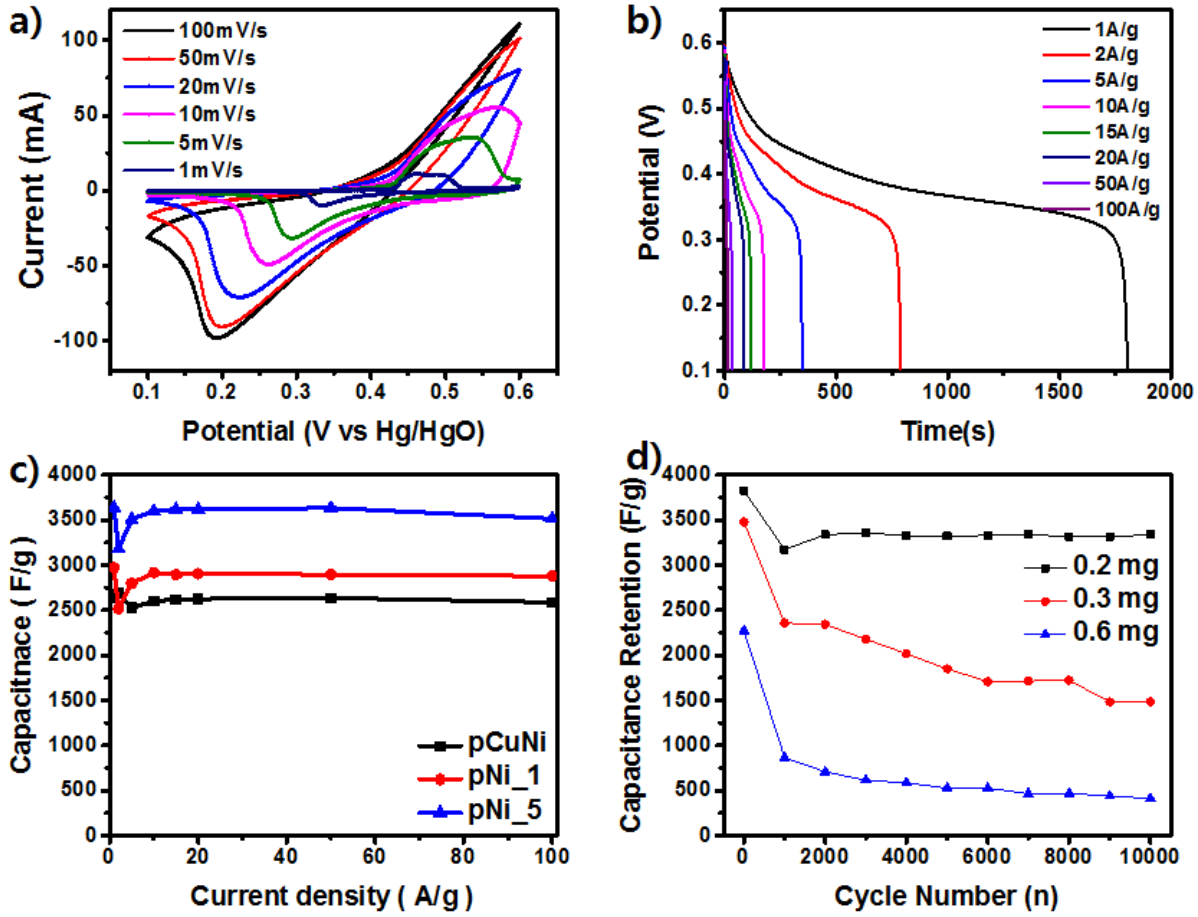

Figure 3.15. Electrochemical characterization of pCuNi, pNi_1 and pNi_5. (a) CV curves of pNi_5 and (b) CD curves of pNi_5. (c) The rate capability of pCuNi, pNi_1 and pNi_5. (d) The weight vary of $Ni(OH)_2$ on pNi_5

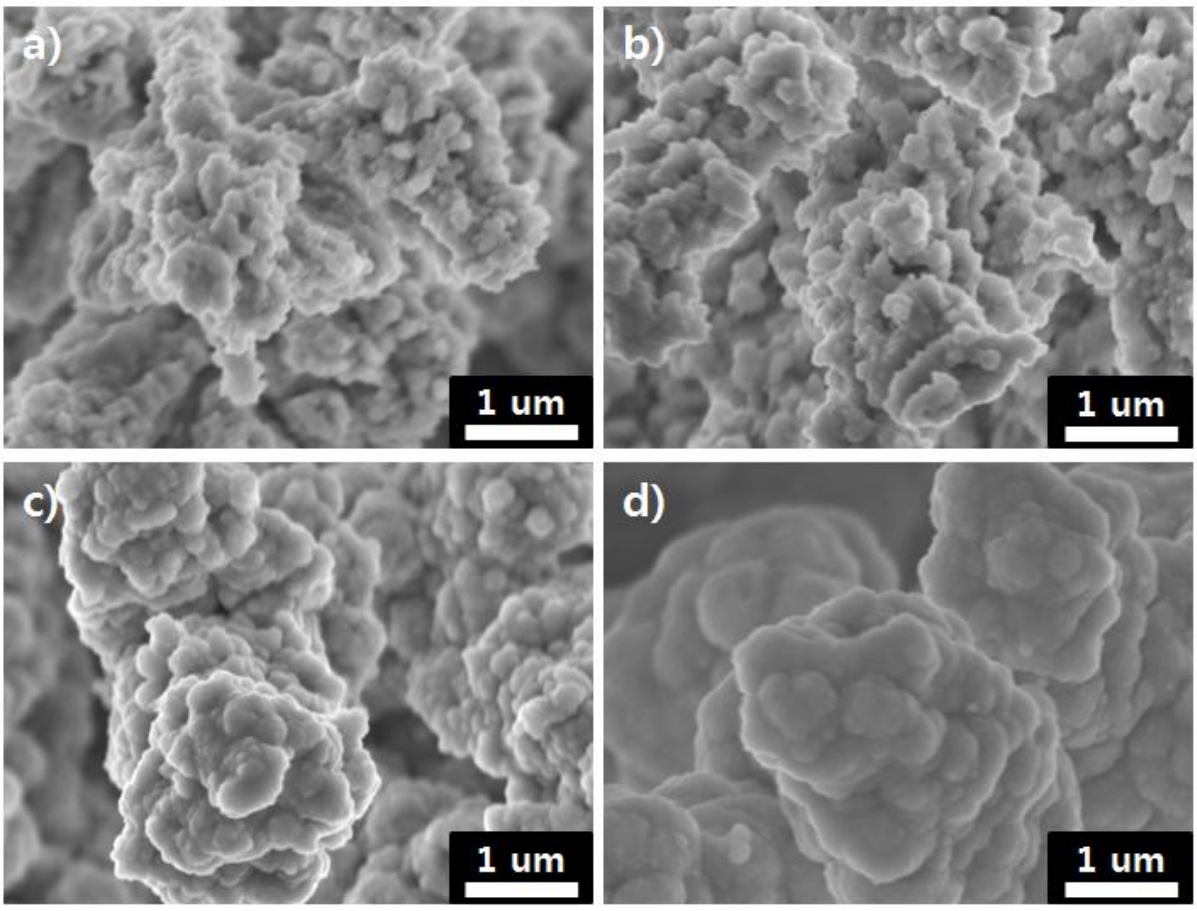

Figure 3.16. SEM images of $Ni(OH)_2$ on pNi_5, (a) 0.2 mg, (b) 0.3 mg, (c) 0.6 mg and (d) 1.0 mg each

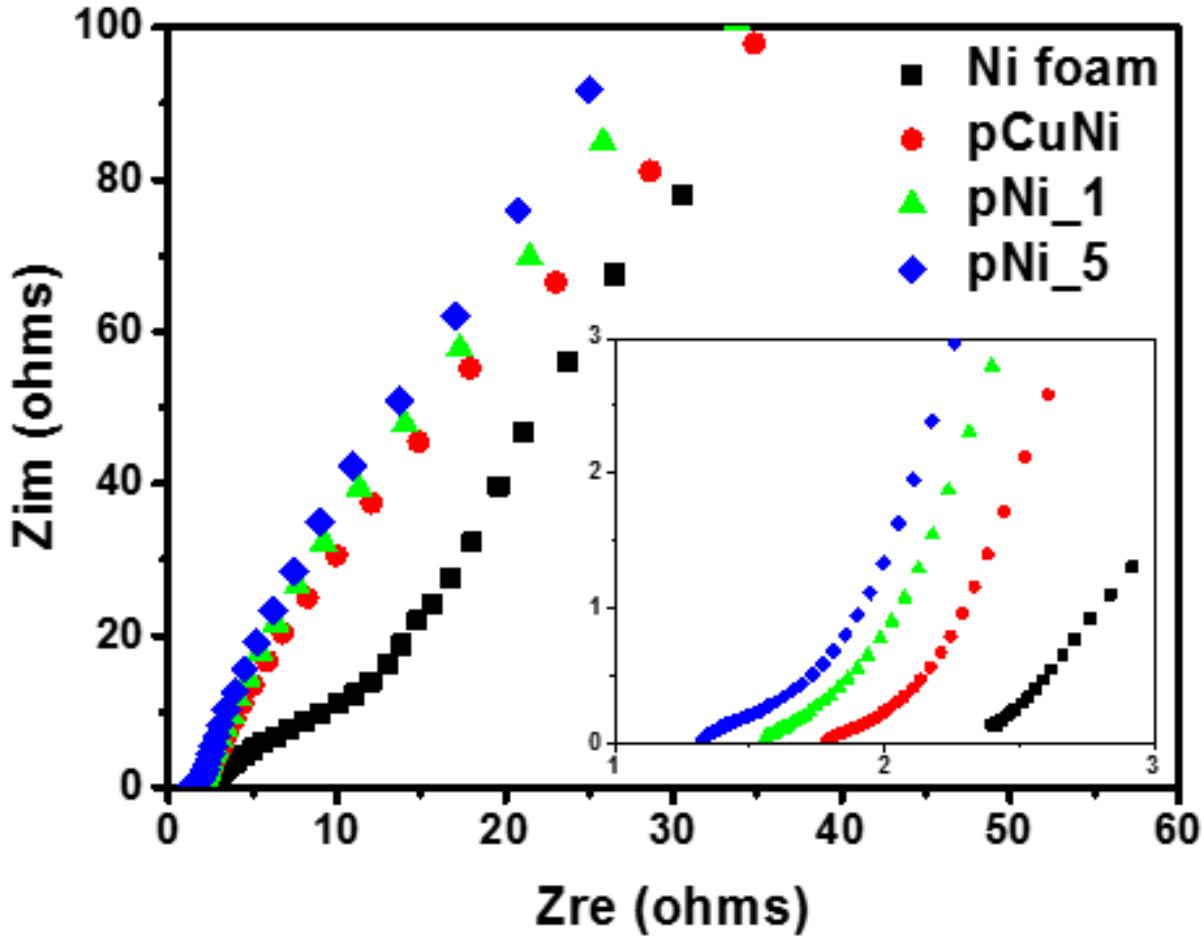

Figure 3.17. Nyquist plot of $Ni(OH)_2$/nickel foam, $Ni(OH)_2$/pCuNi, $Ni(OH)_2$/pNi_1 and $Ni(OH)_2$/pNi_5

3.3 Conclusion

3.3.1 $Ni(OH)_2$/C/pCu

In summary, by using the 3D current collector, overall capacitances were dramatically increased due to its high surface area and short electron pathway. To make pCu, copper was deposited on the cleaned nickel plate at the current density of 3 A/cm^2 for 30 s. Also small contact resistance and charge transfer resistance were induced from the 3D current collector. However in case of the pCu current collector, due to the instability of the copper, additional treatment which is carbon coating using the glucose solution with heating in the inert condition. By coating the carbon layer outside of the pCu, the stability was increased. The electrochemical properties of the as-prepared sample was superior than the conventional $Ni(OH)_2$ based capacitor and commercial nickel foam current collector capacitor.

3.3.2 $Ni(OH)_2$/pNi series

First pCuNi was deposited on the cleaned nickel plate, similar to the pCu. But in case of pCuNi, copper and nickel were co-deposited at the current densitiy of 3 A/cm^2 for 150 s. Deposited pCuNi was used as a current collector itself and for the base material of the pNi_1 and pNi_5. For the pNi_1 and pNi_5, pCuNi was etched in the 0.1 M ammonium persulfate for 1 m and 5 m. The surface area of the etched samples were increased due to the remove of copper. In case of pNi_5, the surface area was increase from 0.9 to 2.0. The specific capacitance of the pNi_5 was highest among the synthesized series, and it is supported by contact resistance and charge transfer resistance. Rs and Rct value of pNi was smallest among the as-prepared samples.

By making the thin film type of supercapacitor on the synthesized 3D current collector, cheap and superior performance capacitor can be made.

3.5 References

1. Wang, G.; Zhang, L.; Zhang, J., A review of electrode materials for electrochemical supercapacitors. *Chemical Society reviews* **2012,** *41* (2), 797-828.
2. Kundu, M.; Liu, L., Direct growth of mesoporous MnO2 nanosheet arrays on nickel foam current collectors for high-performance pseudocapacitors. *Journal of Power Sources* **2013,** *243*, 676-681.
3. Huang, H.; Tang, Y.; Xu, L.; Tang, S.; Du, Y., Direct formation of reduced graphene oxide and 3D lightweight nickel network composite foam by hydrohalic acids and its application for high-performance supercapacitors. *ACS applied materials & interfaces* **2014,** *6* (13), 10248-57.
4. Zheng, C.; Zhang, J.; Zhang, Q.; You, B.; Chen, G., Three dimensional Ni foam-supported graphene oxide for binder-free pseudocapacitor. *Electrochimica Acta* **2015,** *152*, 216-221.
5. Yin, J. L.; Park, J. Y., A nickel foam supported copper core/nickel oxide shell composite for supercapacitor applications. *Microporous and Mesoporous Materials* **2014,** *200*, 61-67.
6. Xiong, X.; Ding, D.; Chen, D.; Waller, G.; Bu, Y.; Wang, Z.; Liu, M., Three-dimensional ultrathin Ni(OH)2 nanosheets grown on nickel foam for high-performance supercapacitors. *Nano Energy* **2015,** *11*, 154-161.
7. Wang, T.; Guo, Y.; Zhao, B.; Yu, S.; Yang, H.-P.; Lu, D.; Fu, X.-Z.; Sun, R.; Wong, C.-P., NiCo2O4 nanosheets in-situ grown on three dimensional porous Ni film current collectors as integrated electrodes for high-performance supercapacitors. *Journal of Power Sources* **2015,** *286*, 371-379.
8. Ying Li, W.-Z. J., Yan-Yan Song, and Xing-Hua Xia*, Sperhydrophobicity of 3D porous copper films perpared using the hydrogen bubble dynamic template. *Chem. Mater.* **2007,** *19*, 7.

Acknowledgement

먼저 지도교수님이신 장지현 교수님과 committee로써 졸업 심사에 힘써주신 나명수 교수님과 고현협 교수님 감사합니다.

그리고 도움을 주신 모든 분 들께 감사의 말씀 전합니다.